



Double- K -hole resonances in single photoionization of He-like B^{3+} ions

A. Müller ^{*}, P.-M. Hillenbrand , S.-X. Wang , and S. Schippers 
I. Physikalisches Institut, Justus-Liebig-Universität Gießen, 35392 Giessen, Germany


E. Lindroth 
Department of Physics, Stockholm University, Alba Nova University Center, 106 91 Stockholm, Sweden

F. Trinter 
Molecular Physics, Fritz-Haber-Institut der Max-Planck-Gesellschaft, 14195 Berlin, Germany

J. Seltmann 
Deutsches Elektronen-Synchrotron (DESY), 22607 Hamburg, Germany

S. Reinhardt  and M. Martins 
Institut für Experimentalphysik, Universität Hamburg, 22761 Hamburg, Germany

A. S. Kheifets 
Research School of Physics, The Australian National University, Canberra, ACT 2601, Australia

I. Bray 
Department of Physics and Astronomy, Curtin University, Perth, WA 6845, Australia
(Dated: January 7, 2025)

Within a joint experimental and theoretical research project, single photoionization of He-like B^{3+} ions was investigated in the energy range from approximately 250 to 1200 eV. With the parent-ion beam in the experiment containing both $1s^2\ ^1S$ ground-state and $1s2s\ ^3S$ metastable B^{3+} ions, double-core-hole resonances could be studied. Two series of hollow resonant states were observed, one populated by K -shell double excitation $1s^2\ ^1S \rightarrow 2\ell n\ell'\ ^1P$ ($\ell = s, p; \ell' = p, s; n = 2, 3, \dots, 6$) at photon energies up to about 510 eV, the other by K -shell single excitation $1s2s\ ^3S \rightarrow 2\ell n\ell'\ ^3P$ ($\ell = s, p; \ell' = p, s; n = 2, 3, \dots, 6$) at energies up to about 310 eV. High resolving powers up to approximately 29000 were achieved. The relativistic many-body perturbation theory was employed to determine level-to-level cross sections for K -shell excitation with subsequent autoionization. The resonance energies were calculated with inclusion of electron correlation and radiative contributions. The energy uncertainties of the most prominent resonances are estimated to be below ± 1 meV. Convergent close coupling (CCC) calculations provided single-photoionization cross sections σ_{34} for B^{3+} including the resonant and non-resonant channels. Apart from the resonances, σ_{34} is dominated by direct ionization in the investigated energy range. The contribution σ_{34}^{dir} of the latter process to σ_{34} was separately determined by using the random-phase approximation with exchange and relativistic Hartree-Fock calculations which agree very well with previous calculations. Direct ionization of one electron accompanied by excitation of the remaining electron was treated by the CCC theory and found to be a minor contribution to σ_{34} .

I. INTRODUCTION

Double-core-hole (DCH) states are of outstanding importance both from a fundamental physics point of view and with respect to applications, e.g., in molecular structure and dynamics studies. DCH states with very short lifetimes enabling detailed time-resolved spectroscopy in molecules [1, 2] have received increasing attention with the advent of x-ray free-electron lasers [3]. These light sources can provide x-ray beams with very high brightness as well as ultrashort pulse durations and, therefore, DCH states can be produced with relatively high yields by single or sequential double photoabsorption and used

to investigate the properties of molecules (see, for example, Refs. [4–6] and references therein).

Due to their exotic nature and, in particular, the delicate effects of electron-electron correlation, double- K -shell vacancies in atoms have been a topic of high interest over many decades. Correlation effects govern the birth, life, and death of DCH states. Therefore, understanding the mechanisms for their production, the exact excitation energies, as well as the decay processes and associated lifetimes provides stimulating challenges for experiment and theory. Few-electron systems are particularly interesting because theoretical approaches can produce very accurate results [7–10] that often surpass experimental precision.

The most fundamental DCH states are produced by double excitations in He-like systems. Pioneering work by Madden and Codling [11] on double excitation of neu-

* Alfred.Mueller@physik.jlug.de

tral helium by a single photon producing autoionizing empty- K -shell states opened the door to an unmatched flow of high-impact experimental and theoretical publications on doubly excited helium atoms and DCH states of atoms in general [10, 12–20] identifying just a few examples here with numerous references to previous high-quality investigations.

Double- K -shell vacancies in He-like systems can be prepared in several different ways. Madden and Codling used synchrotron light for the one-photon double excitation of helium atoms [11]. Different from this very controlled resonant production of autoionizing two-electron levels, the same states can be populated by charged-particle impact on He-like atoms [21–24], by ion-atom or ion-molecule collisions [25–29] as well as by multiple collisions in beam-foil experiments (see, e.g., Refs. [30, 31]) or in plasma environments [32].

In contrast to the extensive investigations on neutral He, experimental studies on the controlled production of He-like ions with empty K shells under single-collision conditions are less numerous. Experimental access to doubly excited states in He-like ions with an outstanding potential of spectroscopic precision is possible via dielectronic recombination in collisions of H-like ions with electrons [33–36] and electron-impact K -shell excitation of $1s2s$ metastable He-like ions [37, 38]. The electron-energy spread in such experiments is limited by electron space-charge and kinematic effects in beams of fast particles resulting in resolving powers $E/\Delta E$ of the order of 1000 for studies of double- K -vacancy levels.

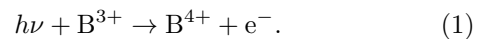
High-resolution detection of decay products from intermediate doubly excited states produced in ion-atom or ion-molecule collisions can provide detailed information, e.g., by spectroscopy of emitted Auger electrons [26, 27, 29], however, typical resolving powers of approximately 300 to 500 mark the inherent limitations of the early experiments. Better resolution can be achieved with optical instruments detecting photons emitted from doubly excited states. Resolving powers in the range 1000 to 2000 have been reached (see, e.g., Ref. [31]). An exceptionally high resolution was achieved with electron spectroscopy of doubly excited states in the Li^+ ion which could be populated starting from neutral Li [39]. The maximum resolving power reached in this experiment was of the order of 1600. Another high-resolution access to doubly excited states in He-like ions is provided by the dual-laser-plasma technique [32] employing optical spectrometers. Observations of $n\ell n'\ell'$ states were made for Li^+ with resolving powers between 1500 and 1900 [40, 41] and for Be^{2+} with $E/\Delta E = 2200$ [42].

Much better resolution is achievable by excitation with narrow-bandwidth photon beams in experiments employing merged beams of photons and ions. However, the controlled production of doubly excited states starting from He-like ions by a single photon is very challenging due to low cross sections for double excitation and low densities of He-like ions in colliding-beams experiments. So far, only two experiments on photoproduction of doubly

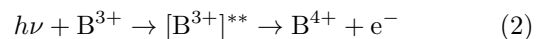
excited He-like ions by employing the photon-ion merged-beams technique have been published. In one of the measurements, single ionization of ground-state Li^+ ions was investigated [43] where doubly excited states were observed with resolving powers up to 13000. Absolute cross sections for direct photo-double-excitation of $\text{Li}^+(1s^2\ ^1S)$ were measured. In a second experiment of the same kind, cross sections for direct single excitation of the K shell of metastable $\text{C}^{4+}(1s2s\ ^3S)$ were determined [44]. Resolving powers up to almost 26000 could be achieved in the spectroscopy of doubly excited He-like C^{4+} . This was sufficient, e.g., for separating the fine structure within the resonantly excited $\text{C}^{4+}(2s2p\ ^3P)$ term that decays by an Auger process to $\text{C}^{5+} + e^-$. In the experiments, the C^{5+} product ions were detected as a function of the incident-photon energy.

Beside the high photon flux available at the third-generation synchrotron light source employed in the experiment and the relatively large cross sections for single K -shell excitation necessary to produce doubly excited levels, one other effect helped with resolving the fine structure of doubly excited resonances in He-like carbon: by starting from the $1s2s\ ^3S$ level of long-lived C^{4+} that already carries a single K vacancy in the initial state, the excitation of the second K -shell electron leads to 3P DCH states. These live much longer and have much smaller lifetime widths than the 1P DCH states that can be excited by one photon from the $1s^2\ ^1S$ ground level. In the present work, we find a lifetime of the $2s2p\ ^3P$ levels in B^{3+} ions that is more than a factor of 10 longer than that of $2s2p\ ^1P$. Clearly, not all DCH states have very short lifetimes as needed for fast time-resolved spectroscopy of molecules. Long lifetime means small natural width and thus facilitates high-resolution measurements with relatively low but monochromatized photon flux without losing too much signal.

In this paper, we present measured yields of B^{4+} ions arising from the absorption of single photons by B^{3+} ions



The ions were provided in the form of a mass-and-charge-analyzed beam. In a photon-ion merged-beams arrangement, the product ions were charge analyzed and counted as a function of photon energy while the photon flux and the ion current were monitored for normalization of the signal. The observed B^{4+} final charge state of the ions can result from different reaction channels, direct, non-resonant, single photoionization with removal of one of the two electrons and an indirect process



where, in a first step, an intermediate autoionizing (double- K -vacancy) state is formed by photoexcitation and, in a second step, the doubly excited intermediate state decays by an Auger process in which an electron is ejected.

The parent ions used in the experiment are produced in the relatively hot plasma of an electron cyclotron res-

onance ion source (ECRIS) where excited states of B^{3+} are also populated. The extracted ion beam contains B^{3+} ions both in the $1s^2\ ^1S$ ground state and in the long-lived metastable $1s2s\ ^3S$ K -shell excited level. Hence, the yield spectrum that is measured in the photon-energy range from approximately 250 to 1200 eV contains contributions from both initial levels. Similar to astrophysical observations or the spectroscopy of earth-bound radiation sources where complex mixtures of different chemical elements in atomic or molecular form and in different charge states are present, the contributions of the different components can be disentangled on the basis of their characteristic-energy fingerprints. In particular, in the present experiment two series of doubly excited states $nln'l'\ ^1P$ and $nln'l'\ ^3P$ with $n, n' \geq 2$ could be observed with high resolution. Their origins are clearly distinguished by their resonance energies. Resonance parameters of the strongest resonances in the single-ionization cross section were determined from the experimental spectra and by using state-of-the-art theoretical methods. Theory and experiment are in very good agreement.

The present paper is organized as follows. Next to this introduction, in Sec. II, the experimental procedures are outlined. In Sec. III, the theoretical approaches are briefly described. Sec. IV summarizes the theoretical results and Sec. V discusses normalization procedures based on theory by which the experimental results are put on an absolute scale. Sec. VI presents the experimental results and compares them with theory. The paper ends with a summary (Sec. VII) and acknowledgements (Sec. VIII).

II. EXPERIMENTAL PROCEDURES

The present experiments were conducted at the soft-x-ray beamline P04 [45] of the synchrotron lightsource PETRA III [46] operated by DESY in Hamburg, Germany. The permanent endstation PIPE (Photon-Ion Spectrometer at PETRA III) [47] of beamline P04 provided the complete experimental setup for the measurements which employed the photon-ion merged-beams technique [48] for the determination of relative cross sections for single ionization of B^{3+} ions by single photons with energies between approximately 250 and 1200 eV. The experimental procedures for the measurement of absolute cross sections at PIPE have been previously described in great detail [49, 50]. Therefore, the present description only summarizes the experimental background of the present project and especially provides the specific details of the present experiments.

A permanent-magnet ECRIS [51] was operated with BF_3 gas to produce the desired B^{3+} ions. Positive ions generated in the ECRIS plasma were extracted and accelerated towards ground potential by a static acceleration voltage $U_{acc} = +6000$ V applied to the plasma chamber. An ion beam was formed by suitable electrostatic

focusing elements. The B^{3+} ions in the beam had an energy of 18 keV and a velocity $v_{ion} = 5.62 \times 10^7$ cm/s when traversing a magnetic analyzer field that filtered the $^{11}B^{3+}$ component from the numerous other ingredients of the ion inventory extracted from the ECRIS. The beam of mass-and-charge-selected $^{11}B^{3+}$ ions was collimated to a diameter of about 1 mm and merged with the counter-propagating photon beam provided by beamline P04. Photoionized product ions, B^{4+} , were separated from the parent-ion beam by a second magnet and transported to a single-particle detector with almost 100% counting efficiency. The parent ions were collected by a large Faraday cup inside the second magnet's vacuum chamber and their electrical current was measured by a sensitive electrometer. The flux of the transmitted photon beam was recorded by a calibrated photodiode. Typical $^{11}B^{3+}$ beam currents in the interaction region were between 2 and 3 nA.

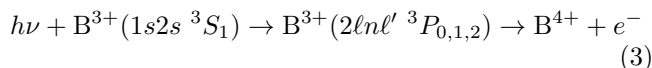
A newly installed blazed grating with 400 lines per mm delivered a very high photon flux of more than 10^{14} photons per second at a photon energy $E_{ph} = 450$ eV and a monochromator exit-slit width of 1000 μm corresponding to a photon-energy bandwidth of approximately 620 meV. The product-ion detector recorded 20 to 25 counts per second (off-resonance) under these conditions. The rate of dark counts was measured to be 0.017(1) Hz where the number in parentheses is the uncertainty of the preceding last digit. The photons did not produce background. Thus, the background under the B^{4+} signal that mainly originates from electron-stripping collisions of the ions in the residual gas almost exclusively depended on the current of incident parent ions and amounted to about 0.2 Hz/nA. The background was subtracted to obtain relative apparent cross sections σ_{34}^{app} for net single photoionization of B^{3+} ions (for further explanation, see the end of this section).

The magnetically filtered parent $^{11}B^{3+}$ ion beam consisted of two components: $^{11}B^{3+}(1s^2\ ^1S_0)$ ground-level and long-lived $^{11}B^{3+}(1s2s\ ^3S_1)$ excited-level ions with a lifetime of 149 μs [52]. Hence, ionization signals from both beam components had to be expected. The fraction f of metastable ions in the parent-ion beam was not *a priori* known. In a previous experiment studying electron-impact ionization of B^{3+} ions from an identical ECRIS, a fraction $f = 0.105$ was derived [53]. The fraction may vary with the operation mode of the ion source, however, the optimization of B^{3+} ion output and the required high temperature of the source plasma necessary to produce multiply charged ions probably leave little room for changing the metastable fraction of these ions.

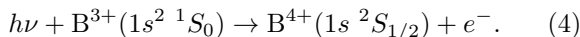
Other parameters that influence the survival of excited states in an ion beam are the flight time between production in the ECRIS and the photoionization in the photon-ion interaction region and the possible quenching by collisions with residual-gas molecules along the flight path. It is not known how long it takes a B^{3+} ion to drift from the ion source plasma to the extraction electrode. This time may be tens of microseconds given the

fact that in neither experiment, indications for the presence of $B^{3+}(1s2s\ ^1S_0)$ metastable ions with a lifetime of $10.86\ \mu\text{s}$ [54] could be found in the parent-ion beam. The flight path between the ion source and the center of the interaction region is approximately 9 m which results in a time of flight of roughly $16\ \mu\text{s}$. Reference [53] stated an upper limit of 1% for the fraction of $1s2s\ ^1S$ parent ions produced in an identical ECRIS. For the present experiment, a $1s2s\ ^3S$ metastable fraction $f = 0.091(16)$ was derived. Since theory was engaged to determine f , the discussion of the procedure employed to quantify the fraction of metastable $B^{3+}(1s2s\ ^3S_1)$ in the parent-ion beam is deferred to Sec. V.

Overview measurements of B^{4+} product-ion yields were conducted by scanning the photon-energy range from 250 eV to 1200 eV in steps of 5 eV with a fixed exit-slit width of $1000\ \mu\text{m}$. In finer scans covering the energy range from 248 to 310 eV, resonances associated with photoexcitation of the metastable ion-beam component and subsequent Auger processes



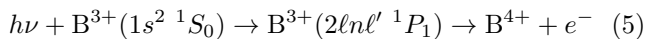
with $\ell = s, p$, $n = 2, 3, 4, 5, 6$, and $\ell' = p, s$ were observed together with the threshold region of direct K -shell photoionization of ground-state ions



Recently, the threshold E_K^{gs} of this process has been calculated to be $259.3744095(15)$ eV [55]. This result provides an extremely accurate energy-calibration reference. For easier orientation in the landscape of the numerous processes that can happen, Table I collects theoretical threshold energies for a number of specified direct ionizations that will be used throughout this paper..

The resonances together with the surrounding smooth part of the apparent cross section σ_{34}^{app} were scanned in a sequence of high-resolution sweeps with photon-energy steps of 0.005 eV at a constant monochromator exit-slit width of $200\ \mu\text{m}$. For the strongest resonance in the whole spectrum, associated with $B^{3+}(2s2p\ ^3P_{0,1,2})$ levels at about 248 eV, detailed scans were performed with a step width of 0.001 eV and an exit-slit width of $8\ \mu\text{m}$. For highest possible resolution, a grating with 1200 lines per mm was employed. In these measurements, the photon flux was down to only 2×10^8 photons per second and the photon-energy resolution was sufficient for partly resolving the triplet structure of the scrutinized 3P resonance term.

Nearly 90% of the parent-ion beam being in the ground state, it was also possible to observe resonances associated with double- K -shell excitation and subsequent Auger decay. This was accomplished for transitions



with $\ell = s, p$, $n = 2, 3, 4, 5, 6$, and $\ell' = p, s$. These 1P resonances are much broader than the 3P resonances populated from the metastable 3S level while their strengths

TABLE I. Threshold energies of specified ionization processes of B^{3+} ions. The numbers were obtained on the basis of the state-of-the-art calculations by Yerokhin *et al.* [55, 64]. Numbers in parentheses indicate the uncertainties of the last two digits. In the upper part of the table, the initial B^{3+} and ionized final B^{4+} levels are given together with the calculated threshold energies in a.u. and eV, respectively. The lower portion of the table shows threshold energies for direct double ionization, i.e., the upper energy limit of the occurrence of resonances.

init. B^{3+}	fin. B^{4+}	threshold (a.u.)	threshold (eV)
$1s^2\ ^1S_0$	$1s\ ^2S_{1/2}$	9.531833739(55)	259.3744095(15)
	$2s\ ^2S_{1/2}$	18.908824556(76)	514.5353284(21)
	$2p\ ^2P_{1/2}$	18.908763075(79)	514.5336555(21)
	$2p\ ^2P_{3/2}$	18.909806352(79)	514.5620445(22)
$1s2s\ ^1S_0$	$1s\ ^2S_{1/2}$	2.078882735(29)	56.56928105(80)
	$2s\ ^2S_{1/2}$	11.455873552(51)	311.7302000(14)
$1s2s\ ^3S_1$	$1s\ ^2S_{1/2}$	2.2345859715(31)	60.806181969(85)
	$2s\ ^2S_{1/2}$	11.611576788(25)	315.96710092(67)
	$2p\ ^2P_{1/2}$	11.611515308(27)	315.96542795(74)
	$2p\ ^2P_{3/2}$	11.612558585(28)	315.99381696(75)
initial B^{3+}	final ion		
$1s^2\ ^1S_0$	B^{5+}	22.034909454(77)	599.6004320(21)
$1s2s\ ^1S_0$	B^{5+}	14.581958450(50)	396.7953036(14)
$1s2s\ ^3S_0$	B^{5+}	14.737661686(25)	401.03220450(68)

are smaller by almost two orders of magnitude. Therefore, in order to obtain sufficient signal rates, the energy range 450 to 515 eV was scanned around the different resonances with lower resolution (400 lines per mm grating, monochromator exit-slit width $400\ \mu\text{m}$) and a wider step width of 0.02 eV. Under these conditions the photon flux at 500 eV was $6.3 \times 10^{13}\ \text{s}^{-1}$.

With the beam of ions counterpropagating the photon beam in the present experiments, a Doppler shift of photon energies by approximately a factor of $1 + v_{\text{ion}}/c = 1.00188$ with the vacuum speed of light c had to be corrected for. The exact treatment of the Doppler correction is provided in Ref. [44] together with remaining associated uncertainties in the experimental determination of the photon energy. The Doppler-corrected photon-energy axis was then calibrated to the double- K -hole resonances calculated within this project with exceptionally high accuracy.

The new reference energies were obtained by employing many-body perturbation theory with inclusion of electron correlation and radiative contributions (see Sec. III A). The uncertainty of almost all of these resonance energies is estimated to be less than 1 meV which is very much smaller than the uncertainties of the often used soft-x-ray calibration reference transitions observable in the photoabsorption by neutral gases such as CO, N_2 , or Ne (see, e.g., Ref. [56]). The present experiment demonstrates the feasibility of much improved photon-energy calibrations on the basis of resonance energies in

the photoionization of He-like B^{3+} ions. Known level energies of heliumlike ions have been employed recently in an attempt to re-determine x-ray transition energies of Ne, CO_2 and SF_6 with improved accuracy [57].

The relative apparent cross sections σ_{34}^{app} for net single ionization of B^{3+} ions were obtained by normalizing the measured count rate of B^{4+} product ions to the photon flux and the measured B^{3+} parent-ion current. “Net single ionization” does not distinguish between different pathways leading to the production of B^{4+} from B^{3+} parent ions by absorption of a single photon. The cross section is “apparent” because it is measured with a mixed parent-ion beam consisting of a ground-state and a metastable-ion component. In particular, it depends on the experiment-specific fraction f of metastable ions in the parent B^{3+} ion beam. The cross section σ_{34}^{app} determined here is “relative” because it is not on an absolute scale since the overlap of the interacting photon and ion beams, the so-called form factor, has not been separately determined. By employing the present theory it is possible to determine f and to put the cross-section contributions on an absolute scale. The details are described in Sec. V.

III. THEORETICAL APPROACHES

In the following subsections, the theoretical methods applied in the present project are briefly described. Detailed accounts of the different approaches can be found in the literature. Therefore, the present descriptions are kept at a minimum.

A. Many-Body Perturbation Theory

The intermediate double- K -hole states observed as resonances in the single ionization of B^{3+} are calculated with relativistic many-body perturbation theory (MBPT) in an all-order formulation including single and double excitations, as described by Salomonson and Öster [58]. This means that all types of excitations that can occur in a pure two-electron system are accounted for. The B^{3+} ion is placed in a spherical box within which a discrete radial grid is used. Diagonalization of the discretized hydrogen-like Dirac Hamiltonian gives a discrete basis set for each spin-angular symmetry (defined by ℓ_j) that is complete on the grid chosen. The basis set is then used to construct correlated wave functions to all orders in the perturbation expansion of the electron-electron interaction. Here, both the Coulomb and the Breit interaction are accounted for. The perturbation expansion is constructed from an *extended model space* [59] whenever a state is dominated by two or more nearly degenerate configurations. An example is the $2s2p\ ^3P_1$ state which in jj -coupling has major contributions both from the $2s2p_{1/2}$ and the $2s2p_{3/2}$ configurations. This is a common scenario in jj -coupling, but also for doubly excited states in

general.

A multipole expansion of the electron-electron interaction is used, making the method applicable to many-electron atoms in general. In the present calculations, the expansion allows for inclusion of all partial waves up to $\ell_{\max} = 10$ for the $2\ell n\ell'$, $n \leq 3$, resonance groups, $\ell_{\max} = 7$ for the $2\ell 4\ell'$ resonance group, and $\ell_{\max} = 6$ for the higher resonances. The convergence rate with respect to ℓ_{\max} is in general considerably faster for the triplet than for the singlet states. The rate was investigated for the $2\ell 2\ell'$ and $2\ell 3\ell'$ resonance groups. For the latter group, the calculations gave convergence rates approximately proportional to ℓ_{\max}^{-6} for the triplet and ℓ_{\max}^{-4} for the singlet states, that is, with increasing ℓ_{\max} the changes of the corrections to the level energies become smaller proportional to ℓ_{\max}^{-6} and ℓ_{\max}^{-4} , respectively. The same behavior was found for the $2\ell 2\ell'$ resonance group with the exception of the $2s2p\ ^1P_1$ state which converges considerably faster than all the other states. In summary, it is found that contributions from $\ell_{\max} > 10$ affect the triplet resonances by less than 0.1 meV, while some of the singlet resonances are affected on the 1 meV level.

When perturbation theory is applied to autoionizing states it is obvious that the use of a discrete basis set will cause problems close to the poles in the energy denominator. A complex scaling of the radial coordinates can, however, solve this problem. The present treatment follows the method employed by Lindroth [60] for the calculation of doubly excited levels in the helium atom, and later for a number of Be-like ions (see, e.g., Ref. [61]). The method yields complex energies for the autoionizing states, where the imaginary part corresponds to the half-life time (due to Coulombic decay) of the state. The decay rates due to photon emission are calculated from the dipole matrix elements between the doubly excited states and the $1sn\ell\ ^3L_J$ states with $n \leq 4$ for the resonance groups $2\ell n\ell'$, $n \leq 4$, and $n \leq 6$ for the higher groups. For details see Ref. [62]. The radiative decay rates of all the considered doubly excited states are completely dominated (with contributions of more than 99%) by photoemission events that require one-electron transitions only. For the underlying theory of complex rotation (CR) and MBPT the reader is referred to a review by Lindroth and Argenti ([63] and references therein).

To account for the contributions to the energies that originate from the quantization of the electromagnetic field, the tabulation of the corrections to the $n \leq 2$ states of hydrogen-like ions by Yerokhin and Shabaev [64] has been used. Since the resonances are mixtures of configurations such as $2sn\ell$, $2p_{1/2}n\ell'$, and $2p_{3/2}n\ell''$, the correction to each such configuration is multiplied with its fraction in the mixture to estimate the effect on the resonance energies. The contribution to the $2s$ level is around 1.6 meV, while the corrections to the $2p$ levels are below 0.1 meV. It is thus only resonances that have a substantial admixture of $2sn\ell$ configurations that will be visibly affected.

The normal mass shift is taken care of by the correc-

tion factor $M/(m_e + M)$ where m_e is the electron rest mass and M the rest mass of the ^{11}B nucleus. The mass-polarization effect (specific mass shift) has also been considered. Calculations of this effect with the non-relativistic formula [65] resulted in shifts of at most 0.1 meV. It is safe to say that mass-polarization shifts of the investigated levels of the heliumlike B^{3+} ion are well below the 1 meV level.

The principle theoretical approach described above has been successfully applied previously to resonance contributions to the single photoionization of $\text{C}^{4+}(1s2s\ ^3S)$ ions [44]. The resonances and the direct-ionization continuum were calculated separately and then added according to Eq. 11 in Ref. [44]. There, the total energies of the initial states were taken from previous results obtained by Drake [7] who used highly correlated non-relativistic wave functions of Hylleraas type to calculate ionization energies. Relativistic and radiative corrections were subsequently treated as perturbations. The calculation is thus very different from the one presented here. Yet, the two calculations agree with one another within 0.5 meV.

The salient feature in the MBPT approach used here is that each calculation is done for a limited number of doubly excited states, defined by a so-called model space, and all the configuration outside this space is included through an iterative procedure. It is then possible to use a very large configuration space. The drawback is that the iterative procedure might not converge, however, this is not really a problem in multiply charged ions with few electrons where the n -manifolds such as, for example, $2\ell_j n \ell'_j$, are well separated. The radial basis is complete on the chosen grid, and can thus be saturated, and the numerical uncertainty associated with the grid is well below the main sources of uncertainty. The main sources of uncertainty of MBPT results are instead 1) the partial wave expansion, and the convergence when including higher angular momenta (here $\ell_{\text{max}} = 10$ is used for the lowest energy resonances) and 2) physics beyond the Dirac equation.

B. Convergent Close Coupling Approach

The convergent close coupling (CCC) approach to calculating single and double photoionization of helium and helium-like ions was developed by Kheifets and Bray [66, 67]. A broader review is available [68], as are some recent developments focusing on the near-threshold behavior [69]. Briefly, upon photoabsorption the final photoelectron-ion interaction is calculated by expanding the ionic wave functions in an orthogonal Laguerre basis. For each orbital angular momentum $\ell \leq \ell_{\text{max}}$, this basis has the parameter basis size N_ℓ and exponential fall-off λ_ℓ . We rely on the completeness of the basis to ensure that convergence, to a desired precision, is obtained by simply increasing the basis sizes. In order to reduce the number of free parameters, we typically set

$N_\ell = N_0 - \ell$ and $\lambda_\ell = \lambda$, thereby reducing convergence testing to just the three parameters ℓ_{max} , λ , and N_0 . The photoelectron-ion wave function is then obtained via the CCC method, which solves the resulting close-coupling equations in momentum space. The photoionization amplitude is formed by evaluating the dipole operator between the target ground state and the CCC-calculated wave function. This is evaluated in the three gauges of length, velocity, and acceleration. When both the initial B^{3+} target state wave function and the CCC-calculated final total wave function of $e^- - \text{B}^{4+}$ are sufficiently accurate, then the three forms yield indistinguishable results.

In the present case of $\gamma - \text{B}^{3+}$ interaction, the hydrogen-like B^{4+} wave functions are obtained by setting $\ell_{\text{max}} = 4$, $\lambda = 3$, and $N_0 = 35$. Only open states are retained as the contribution of closed states was found to be insignificant. This means the size of the calculations rapidly increases with photon energy. Nevertheless, with modern computational resources the calculations take no more than just a few minutes per photon energy. The velocity form is presented throughout, but the others are barely distinguishable except for the direct-ionization base level of the cross section for direct removal of a $2s$ electron from $\text{B}^{3+}(1s2s\ ^3S)$ where differences of up to about 23% between the three gauges are found.

The accuracy of the CCC results depends critically on the accuracy of the wave functions of the initial and final states of the interaction process under consideration. The quality of the wave functions relies on the size and suitability of the basis set employed for their construction. Since the computational efforts for calculating cross sections rapidly increase with the basis size, limitations of this size are inevitable. The description of the initial state of the target B^{3+} within the existing computational constraints is more difficult for the metastable $1s2s\ ^3S$ than for the $1s^2\ ^1S$ ground level. Expanding the basis for constructing a better wave function for the metastable level of B^{3+} would require an unmanageable effort. Such limitations are the main reason for inaccuracies of CCC results.

C. Relativistic Hartree-Fock Approach

The B^{3+} K -shell photoabsorption cross sections for the $1s^2\ ^1S$ and $1s2s\ ^3S$ initial states were modeled by *ab initio* configuration-interaction (CI) calculations on the basis of the Hartree-Fock method with relativistic extensions (HFR) applying the Cowan code [70]. The theoretical approach has been described in detail previously [71].

For describing the B^{3+} initial states, the CI expansion was chosen to include the configurations $1s^2$, $1s2s$, $2s^2$, and $2p^2$. The direct photo single-ionization cross sections for the removal of one $1s$ electron from $\text{B}^{3+}(1s^2\ ^1S)$ was derived from the dipole matrix elements $\langle \Psi_{e\ell} | er | \Psi_{1s^2\ ^1S} \rangle$ where er is the dipole operator. The wave function $\Psi_{e\ell}$ represents the residual B^{4+} ion and the ionized electron with kinetic energy ϵ and angular momentum $\ell = p$.

The direct removal of the $1s$ or the $2s$ electron from $B^{3+}(1s2s\ ^3S)$ was treated accordingly.

D. Random-Phase Approximation with Exchange

The development of the random-phase approximation (RPA) was originally directed to describe phenomena in infinite materials [72, 73]. Advances in the computing technologies allowed the application of the RPA also to finite systems such as atoms [74]. Advanced calculations additionally consider the exchange effects resulting from the fact that electrons cannot be distinguished from one another. The associated theory is the random-phase approximation with exchange (RPAE) [74, 75], which was applied here to calculate cross sections for direct $1s$ and $2s$ photoionization of the $B^{3+}(1s^2\ ^1S)$ and $B^{3+}(1s2s\ ^3S)$ ions investigated in the present experiments.

IV. THEORETICAL RESULTS

In this section, an overview of the theoretical results is provided with emphasis on their applicability to the present measurements. Comparisons with previous theoretical work are presented where suitable data are available.

The cross section σ_{34} for net single ionization of B^{3+} comprises several reaction channels. The most straightforward concept of photoionization is the direct removal of a single electron (the photoelectric effect) from the parent ion as described by Eq. 4. When starting from the ground state, it is described by the cross section σ_{34}^{gs-dir} . For the metastable B^{3+} ion, the corresponding cross section is σ_{34}^{ms-dir} . Another direct process that may occur is the removal of one electron accompanied by excitation (shake-up) of the other electron to an excited level of the remaining B^{4+} ion. In the present context, cross sections σ_{34}^{gs-n} and σ_{34}^{ms-n} for direct K -shell ionization plus excitation to the main shell with principal quantum number n were calculated for ground-state and metastable B^{3+} ions, respectively, using the CCC approach. Such two-electron processes have been investigated previously [67] and found to be of minor importance for the net ionization of He-like ions. The further discussion of theoretical results in this section (see subsection IV C) shows that ionization-excitation (IE) can be safely neglected in the assessment of σ_{34} also for B^{3+} ions. Nevertheless, it is elucidating to see how much the cross sections σ_{34}^{gs-n} and σ_{34}^{ms-n} are influenced by DCH resonances.

As the last sentence of the preceding paragraph suggests, indirect ionization may occur in addition to the direct non-resonant processes contributing to σ_{34} . Indirect ionization proceeds via the excitation of intermediate autoionizing levels as described by Eqs. 3 and 5. In the energy range of the present investigation, such resonances are populated by two-electron excitations of ground-state B^{3+} or by single K -shell excitation of metastable B^{3+} .

The resulting doubly excited states decay with high probability by the emission of an Auger electron. In the present paper, the associated cross sections are σ_{34}^{gs-res} for ground-level B^{3+} and σ_{34}^{ms-res} for the metastable heliumlike boron ions. The cross sections for IE to highly excited n shells of the hydrogenlike B^{4+} ionization products are also influenced by resonances. With increasing principal quantum numbers n , the IE cross sections reveal increasing relative contributions of doubly excited B^{3+} resonances with both electrons in high Rydberg states where the Auger decay populates highly excited $B^{4+}(n\ell)$ levels.

A. Direct single photoionization

In the energy range explored in this work, net single ionization of He-like B^{3+} is dominated by direct K -shell ionization. The cross sections for direct removal of a $1s$ electron from either $B^{3+}(1s^2)$ or $B^{3+}(1s2s)$ can be calculated with good accuracy. The quality of available calculations may be judged by comparing the results of several different theoretical approaches (see Fig. 1 and its inset). The remarkable agreement among the theoretical results provides a very good basis for normalizing experimental cross sections.

Figure 1 shows cross sections σ_{34}^{gs-dir} for direct photoionization of $B^{3+}(1s^2\ ^1S)$ resulting from eight different

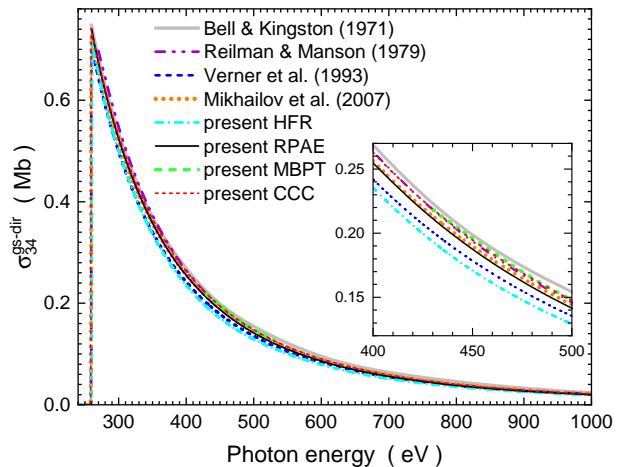


FIG. 1. (color online) Theoretical cross sections σ_{34}^{dir} for direct photoionization of $B^{3+}(1s^2\ ^1S)$. The light-gray solid line is the result obtained by Bell and Kingston [76], the magenta dash-dot-dotted line is from work of Reilman and Manson [77], the blue dashed line is from Verner *et al.* [78], the orange dotted line is the calculation by Mikhailov *et al.* [79], the cyan dash-dotted line is the present HFR result, and the black solid line is the result of the present RPAE theory. Direct single ionization cross sections were also obtained from the present MBPT and CCC calculations by removing the resonance contributions. The green thick dashed line is the MBPT result and the red fine dashed curve is the CCC result. The inset zooms into the energy range 400 to 500 eV.

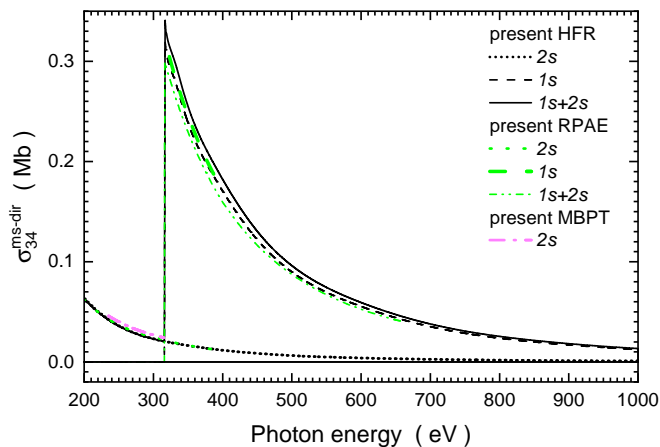


FIG. 2. (color online) Theoretical cross sections for direct photoionization of metastable $B^{3+}(1s2s^3S)$. The present HFR results are shown as black lines, the RPAE results are shown as green lines, and the MBPT direct $2s$ ionization cross section is shown as a magenta dash-dotted line. The solid black curve is the total direct-ionization cross section $\sigma_{34}^{\text{ms-dir}}$, i.e., the sum of the partial cross sections for $2s$ and $1s$ ionization. The black dashed line is the partial cross section $\sigma_{34}^{\text{ms-dir-}1s}$ for direct removal of the $1s$ electron. The black narrow-dotted line is the partial cross section $\sigma_{34}^{\text{ms-dir-}2s}$ for direct removal of the $2s$ electron. The RPAE results for direct $2s$ ionization are represented by the wide-dotted green line, for direct $1s$ ionization by the dash-dot-dotted green line, and for the sum of $1s$ and $2s$ ionization by the thick wide-dashed green line.

theoretical approaches. For He-like B^{3+} in its ground level, $\sigma_{34}^{\text{gs-dir}}$ is identical with the cross section $\sigma_{34}^{\text{gs-dir-}1s}$ of direct K -shell single ionization by a single photon without an additional excitation of the remaining electron. These cross sections have been calculated by a number of different authors. An early result for photoionization of B^{3+} was obtained by Bell and Kingston [76] who derived the cross section from the generalized oscillator strength in the dipole approximation and suitably constructed wave functions for the ground and excited states. Their result is represented by the solid light-gray line in Fig. 1. Extensive tables of cross sections for direct ionization of atoms and ions were generated by Reilman and Manson [77] performing subshell-specific Hartree-Slater central-field calculations. The magenta dash-dot-dotted line shows their result for ground-state B^{3+} . Verner *et al.* [78] performed similarly extensive calculations and tabulated their results in the form of parameters for simple fitting functions. Their calculations are relativistic, and they are based on the self-consistent Hartree-Dirac-Slater potential. Their prediction for direct K -shell ionization of B^{3+} is shown by the blue dashed line. Mikhailov *et al.* [79] generalized the early Stobbe theory [80] and particularly addressed the effects of electron-electron correlation. The thick-dotted orange line is their result. Within the present project, the HFR theory (see Sec. III C) and the RPAE theory

(see Sec. III D) were employed to calculate $\sigma_{34}^{\text{gs-dir-}1s}$ for ground-level B^{3+} . The results are represented by the cyan dash-dotted and black solid lines, respectively. Direct single-ionization cross sections were also obtained by removing the contributions of resonances to the cross sections calculated with the unified-theory MBPT and CCC approaches. The results are displayed in Fig. 1 with the thick dashed green line representing MBPT and the fine dashed red curve representing CCC. All these calculations give almost identical cross sections as Fig. 1 clearly demonstrates.

While direct ionization of $B^{3+}(1s^2^1S)$ involves only a single electron shell, the cross section $\sigma_{34}^{\text{ms-dir}}$ of metastable $B^{3+}(1s2s^3S)$ comprises the two partial cross sections for the $1s$ shell and the $2s$ subshell. Figure 2 displays these two partial cross sections together with their sum $\sigma_{34}^{\text{ms-dir}} = \sigma_{34}^{\text{ms-dir-}1s} + \sigma_{34}^{\text{ms-dir-}2s}$. The partial cross sections for the $1s$ and $2s$ direct-ionization contributions were obtained by employing the present HFR, RPAE, and MBPT approaches. At this point it should be mentioned that the direct and indirect processes, described, e.g., by Eqs. 4 and 5 for ground-state B^{3+} ions, cannot really be treated independently. In the vicinity of resonance contributions, the amplitudes of the two interaction channels can interfere with one another so that the reaction pathways described by Eqs. 4 and 5 cannot be distinguished. This calls for a unified theoretical treatment.

B. Net single photoionization of B^{3+}

Two theoretical approaches were used in the present study to obtain the cross sections for net single photoionization of $B^{3+}(1s^2^1S)$ and $B^{3+}(1s2s^3S)$.

1. $B^{3+}(1s^2^1S)$

The net single-ionization cross section σ_{34}^{gs} calculated using the present CCC theory is shown as the solid blue line in panel (a) of Fig. 3. The same cross section calculated using the present MBPT method is represented by the red solid line in panel (b). The CCC calculations comprise all photoionization contributions that lead from the ground state of B^{3+} to the final charge state B^{4+} . Within the constraints of the chosen Laguerre basis, the CCC theory includes resonances up to very highly excited DCH levels as evidenced by Fig. 4. The unified CCC theory permits calculations of cross sections as a function of photon energy only on a point-by-point basis. This implies that narrow resonances can only be mapped out completely, if the grid of energies is sufficiently dense. Because of the existing constraints in computing resources, the number of energy steps had to be limited in the CCC calculations.

The MBPT method permits derivation of all relevant parameters associated with individual resonances. In or-

TABLE II. Calculated parameters (using MBPT) of the 28 energetically lowest resonance contributions to single photoionization of ground-state $B^{3+}(1s^2\ ^1S)$. The most relevant excited levels are associated with 1P_1 states due to the selection rules for electric-dipole transitions. All levels have a total angular momentum $J = 1$. The first column provides the leading configuration and the associated term of each resonance. The entries in columns 2, 3, and 4 are results for the resonance energies relative to the $B^{3+}(1s^2\ ^1S)$ parent-ion initial level. E_{res} includes the most accurate results with extrapolated contributions of un-calculated high- ℓ partial waves. Several entries in this column are missing because extrapolations for $2\ell n\ell'\ ^1P$ resonances with $n \geq 4$ were not performed. E_{res}^0 represents the resonance energies obtained without extrapolation and E_{res}^* is without the resonance QED corrections (and without extrapolation). Further entries are the natural (life-time) widths Γ , the Fano q parameters [81], the Auger decay rates A_a , the total radiative rates A_r , the branching ratios for Auger decay B_a , and the ionization resonance strengths S_{ion} . Numbers in square brackets are powers of 10.

level	E_{res} eV	E_{res}^0 eV	E_{res}^* eV	Γ eV	q	A_a s^{-1}	A_r s^{-1}	B_a	S_{ion} MbeV
$2s2p\ ^3P$	446.8200	446.8200	446.8184	9.151[-3]	-1.331	1.357[13]	3.307[11]	0.9762	9.755[-8]
$2s2p\ ^1P$	453.1648	453.1660	453.1644	8.442[-2]	-1.833	1.279[14]	3.540[11]	0.9972	5.958[-2]
$2s3p\ ^3P$	487.1025	487.1025	487.1017	3.810[-3]	-1.458	5.566[12]	2.227[11]	0.9615	1.205[-7]
$2s3p\ ^1P$	485.8058	485.8058	485.8050	3.599[-4]	-2.293	3.135[11]	2.333[11]	0.5733	1.267[-4]
$2p3s\ ^3P$	487.4328	487.4328	487.4324	3.207[-4]	-1.804	1.855[11]	3.018[11]	0.3807	4.825[-8]
$2p3s\ ^1P$	489.7694	489.7698	489.7691	3.259[-2]	-1.793	4.923[13]	2.782[11]	0.9944	1.732[-2]
$2p3d\ ^3P$	490.7797	490.7797	490.7793	2.103[-4]	-1.659	1.096[9]	3.184[11]	0.0034	7.559[-10]
$2p3d\ ^1P$	491.7520	491.7529	491.7526	8.539[-4]	-1.316	9.579[11]	3.395[11]	0.7383	8.018[-5]
$2s4p\ ^3P$	499.5273	499.5273	499.5265	1.600[-3]	-1.665	2.228[12]	2.033[11]	0.9164	3.535[-7]
$2s4p\ ^1P$	-	499.1207	499.1199	2.693[-4]	-2.244	1.984[11]	2.107[11]	0.4849	5.979[-5]
$2p4s\ ^3P$	499.8705	499.8705	499.8701	2.686[-4]	-1.767	1.075[11]	3.006[11]	0.2634	1.226[-7]
$2p4s\ ^1P$	-	500.6874	500.6869	1.201[-2]	-2.221	1.792[13]	3.288[11]	0.9820	8.260[-3]
$2p4d\ ^3P$	501.1097	501.1097	501.1093	1.995[-4]	-1.708	2.818[9]	3.002[11]	0.0093	6.669[-9]
$2p4d\ ^1P$	-	501.5018	501.5014	5.234[-4]	-1.280	4.767[11]	3.185[11]	0.5994	2.674[-5]
$2s5p\ ^3P$	505.1085	505.1085	505.108	8.503[-4]	-1.755	1.094[12]	1.976[11]	0.8470	7.308[-7]
$2s5p\ ^1P$	-	504.929	504.928	1.958[-4]	-2.226	1.242[11]	1.733[11]	0.4173	3.051[-5]
$2p5s\ ^3P$	505.3219	505.3219	505.322	2.409[-4]	-1.752	6.376[10]	3.023[11]	0.1742	1.898[-7]
$2p5s/5d\ ^1P/{}^3D$	-	505.709	505.709	3.820[-3]	-3.148	5.457[12]	3.469[11]	0.9402	2.775[-3]
$2p5s/5d\ ^1P/{}^3D$	-	505.701	505.701	3.821[-3]	-1.124	5.451[12]	3.550[11]	0.9388	3.945[-4]
$2p5d\ ^3P$	505.9259	505.92599	505.925	1.974[-4]	-1.716	5.185[9]	2.948[11]	0.0173	2.437[-8]
$2p5d\ ^1P$	-	506.120	506.119	3.674[-4]	-1.251	2.479[11]	3.103[11]	0.4441	8.885[-6]
$2s6p\ ^3P$	508.0743	508.0743	508.073	5.326[-4]	-1.740	6.182[11]	1.910[11]	0.7639	1.128[-6]
$2s6p\ ^1P$	-	507.979	507.978	2.133[-4]	-1.534	8.569[10]	2.383[11]	0.2645	4.443[-6]
$2p6s\ ^3P$	508.2090	508.2090	508.209	2.245[-4]	-1.775	4.291[10]	2.982[11]	0.1258	2.796[-7]
$2p6s/6d\ ^1P/{}^3D$	-	508.426	508.426	2.090[-3]	-2.623	2.826[12]	3.491[11]	0.8900	1.272[-3]
$2p6s/6d\ ^1P/{}^3D$	-	508.417	508.417	2.488[-3]	-1.493	3.429[12]	3.508[11]	0.9072	8.079[-4]
$2p6d\ ^3P$	508.5514	508.5514	508.551	1.936[-4]	-1.853	8.317[9]	2.858[11]	0.0283	7.840[-8]
$2p6d\ ^1P$	-	508.661	508.660	2.966[-4]	-1.346	1.307[11]	3.199[11]	0.2900	4.409[-6]

der to keep the required calculations tractable, the number of individual resonances was restricted to the 28 energetically lowest levels. Because of the limitations of the CCC and MBPT calculations, the resonance contributions shown in Fig. 3 panels (a) and (b) differ from one another. For the 28 resonance levels investigated by the MBPT method, very accurate parameters could be obtained (see Table II). Uncertainties of level energies are estimated to be less than 2 meV for the singlet states $2\ell n\ell'\ ^1P$ with $n \geq 4$ and below ± 1 meV for all other resonances investigated. As discussed in Sec. III A, the summation over higher partial waves generally con-

verges more slowly for the singlet states and we estimate the $2s2p\ ^1P_1$ state to shift downwards by 1.2 meV when $\ell > 10$ is considered, the $2p3s\ ^1P_1$ state to shift downwards by 0.4 meV, and the $2p3d\ ^1P_1$ state to shift downwards by 0.9 meV. For the $2s3p\ ^1P_1$ state as well as for the triplet states the effect is below 0.1 meV. For levels with $n \geq 4$ we estimate that the contributions from higher ℓ values are less than 1 meV for the triplets and less than 2 meV for the singlets.

The role of the parameters in calculating the photoionization cross section has been described in detail previously [44]. The cross section σ_{34}^{gs} shown in Fig. 3 panel (b)

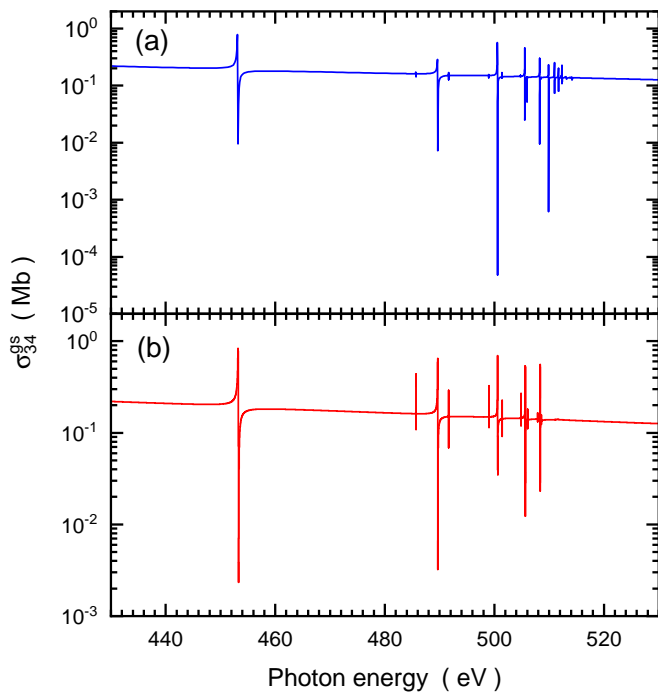


FIG. 3. (color online) Theoretical cross sections σ_{34}^{gs} for net single photoionization of ground-level $\text{B}^{3+}(1s^2 1S)$ ions in the region of double K -shell excitation resonances. Panel (a) presents the result of the present CCC calculations. Panel (b) shows the present MBPT results.

was evaluated by using the parameters provided in Table II. In this table and throughout the present work, the resonances are classified by their leading LS -term. That this classification is meaningful can be deduced, e.g., from Table II where it is evident that the strengths of the $1P$ resonances (last column) are generally larger than those of the triplet resonances (which will not be populated in the non-relativistic limit). This is particularly true for the symmetrically excited resonances. The reason is the size of the term splitting relative to the fine structure. For the lower resonances the fine-structure splitting of the inner electron (~ 0.03 eV) is much smaller than the term splitting: for principal quantum numbers of the first and second electrons $n_1 = 2$ and $n_2 = 3$, respectively, the term splitting is around one eV, and for $(n_1 = 2, n_2 = 4)$, it is a few tenths of an eV. This leads to a singlet-triplet mixing of below one percent in the former case and below ten percent in the latter. For $n_1 = 2$ and $n_2 = 5$ on the other hand, there are cases where the term splitting is smaller than the fine-structure splitting. In this case we see a breakdown of LS coupling as indicated in Table II for the resonances at ~ 505.7 eV.

In general, doubly excited states have to be described, even qualitatively, by a combination of several strongly mixing configurations. One example can be the states dominated by the nearly degenerate $2s4p$, $2p4s$ and $2p4d$ configurations. The present calculation uses a model space consisting of all contributing jj configurations.

The result is then projected onto LS -coupled configurations and named after the leading one. This name should not be taken too seriously. For example, the state labeled $2s4p_{J=1}$ in Table III is in fact 51% $2s4p$, 44% $2p4s$, and 5% $2p4d$. The admixtures are, however, very similar for $J = 0$, $J = 1$, and $J = 2$, and the naïve expectation that the $2s4p$ triplet of states should be below the $2p4s$ triplet, which in turn is below the $2p4d$ triplet, indeed holds as seen in Table III.

Alternative quantum labels have been developed for doubly excited states [82, 83]. In the well established notation ${}_N(K, T)_n^A$ [84] the strongest resonances seen in Table II are classified by ${}_2(0, 1)_n^+$, while nearby states of the same overall symmetry ($1P^o$), which are significantly more narrow and considerably weaker, belong to the ${}_2(1, 0)_n^-$ or ${}_2(-1, 0)_n^0$ series. The dominance of the population of the ${}_2(0, 1)_n^+$ series from the ground state can be explained by so-called propensity rules [12]. In Table III, where the doubly excited states are populated from the $1s2s 3S$ level, the strongest resonances belong to the ${}_2(1, 0)_n^+$ series, but also the ${}_2(0, 1)_n^-$ resonances are prominent in the spectra, cf. Fig. 13. Here it is in fact the $A = -1$ states that are favoured during the population, as predicted by the propensity rules, but their smaller branching ratio for Auger decay results still in the $A = +1$ resonances being the strongest in the spectra. The ${}_N(K, T)_n^A$ labels have some predictive power and are therefore helpful in characterizing the spectrum of doubly excited states in heliumlike systems. Reviews on the physics of two-electron systems have provided detailed explanations of the connection between new correlation quantum numbers and the new theoretical approaches behind them [14, 85]. In the present paper, dealing with the lowest doubly excited levels of heliumlike B^{3+} , we stick to the simple LS labels but also provide assignments with the KT^A classification scheme.

Figure 4 shows the partial cross section $\sigma_{34}^{\text{gs-res}} = \sigma_{34}^{\text{gs}} - \sigma_{34}^{\text{gs-dir}}$. This is the contribution of resonances to net single photoionization associated with doubly excited levels in heliumlike B^{3+} . The spectrum for atomic number $Z = 5$ provided here, corresponds to the data for $Z = 2$ found in a series of previous publications on resonances in the photoionization of neutral He [86–89]. In the present work, autoionizing two-electron levels are characterized by the leading configuration in the LS coupling scheme as mentioned above. The IE thresholds labeled with the principal quantum numbers n of the excited B^{4+} product states clearly mark segments of the ionization resonance spectrum. The strongest resonance contributions are found below the $n = 2$ threshold. With increasing n the resonance series contributing to net single ionization are associated with smaller cross sections.

For a more direct comparison of the results from the present CCC and MBPT calculations, Fig. 5 shows the cross sections σ_{34}^{gs} from both theoretical approaches. The energy range is limited to resonances with the “inner” electron in the $N = 2$ shell and the “outer” electron in

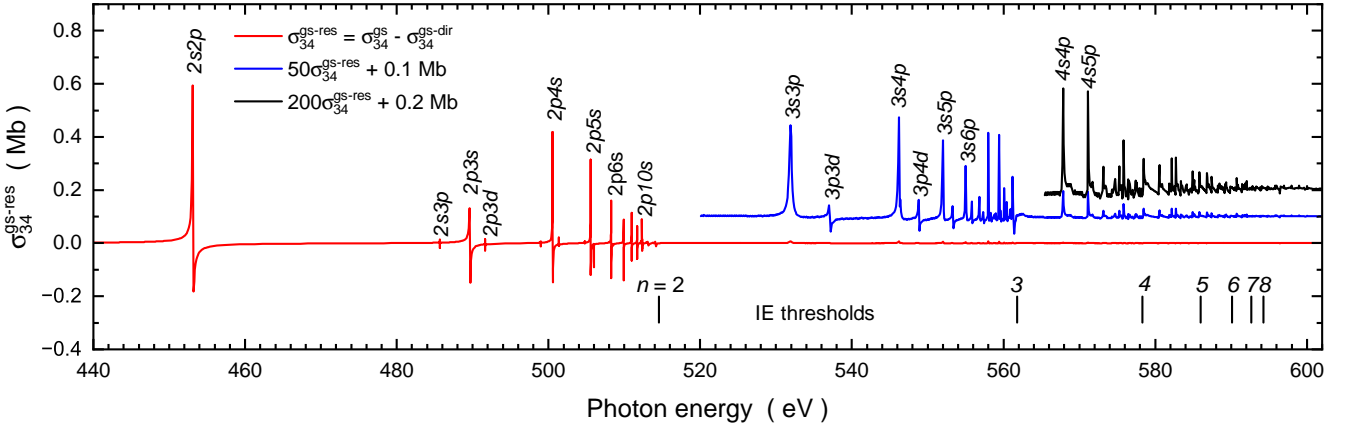


FIG. 4. (color online) Resonance contributions σ_{34}^{gs-res} to the net single photoionization of heliumlike $B^{3+}(1s^2 1S)$ ions obtained by subtracting σ_{34}^{gs-dir} for direct photoionization from CCC calculations of σ_{34}^{gs} . The (red) solid is the overview spectrum of resonances. The next line up (blue) is the same curve multiplied by a factor 50 and offset by 0.1 Mb. The spectrum of resonances was multiplied by a factor 200 and offset by 0.2 Mb to obtain the black line. The most important resonance features are identified by their leading LS configuration. All resonances visible in the spectrum are associated with 1P_1 levels. The vertical bars labeled with numbers n indicate the thresholds for IE processes leading to hydrogenlike B^{4+} in levels with the electron in shells with principal quantum numbers n .

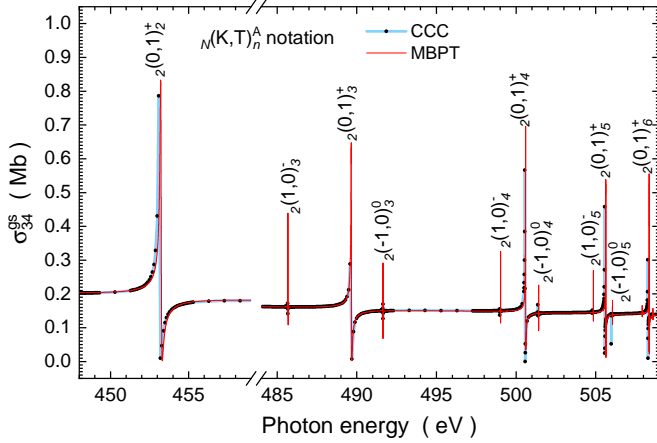


FIG. 5. (color online) Theoretical cross sections σ_{34}^{gs} for net single photoionization of ground-level $B^{3+}(1s^2 1S)$ ions in the energy range below the threshold for ionization with excitation of the remaining electron to the L shell. The black dots connected by a light-blue solid line are the results of the present CCC calculations. The thin solid red line shows the present MBPT results. The resonances are labeled using the $N(K, T)_n^A$ notation.

shell n with $n \geq 2$. The $N(K, T)_n^A$ classification scheme is employed. There is a relatively good overall agreement between the two calculated cross sections. A closer inspection shows, however, that resonance energies do not quite match nor are the maxima and minima of resonance peaks identical. This is particularly true for the very narrow $2(1,0)_n^-$ and $2(-1,0)_n^0$ series of levels. A part of these discrepancies may be attributed to the fact that CCC calculations are only possible at discrete en-

ergies. With a chosen density of grid points, resonance strength may be missed that would otherwise be visible with smaller energy steps in the calculations.

2. $B^{3+}(1s2s 3S)$

The net single-ionization cross section σ_{34}^{ms} calculated using the present CCC theory in the velocity gauge is shown as the dotted cyan line in Fig. 6. In the energy range below the K edge, the calculations in the length, velocity, and acceleration gauges do not fully agree with each other indicating an incomplete representation of the initial state. For comparison, the result associated with the acceleration gauge is shown by the solid red line. The thick light-gray line is the direct-ionization cross section σ_{34}^{ms-dir} obtained by the present HFR calculations.

The step in the cross section at about 315 eV marks the onset of direct K -shell ionization of metastable $B^{3+}(1s2s 3S)$. Below that step are the contributions of direct ionization of the $2s$ subshell and (resonant) single excitation of the K shell. As mentioned in the context of Fig. 3 the CCC calculations did not fully map out individual resonance contributions which would have required a much higher density of energy-dependent cross-section points. Although “incomplete” in that sense, the CCC calculations do show, however, that the resonances at energies above the K edge are very small reaching maxima in the range of 0.1 Mb. These resonances were not observed in the present experiments. They are associated with double excitations of both the $1s$ and the $2s$ electron in the initial $B^{3+}(1s2s 3S)$ ion. In contrast to these double excitations, the strongest resonance below the K edge at about 250 eV is associated with single

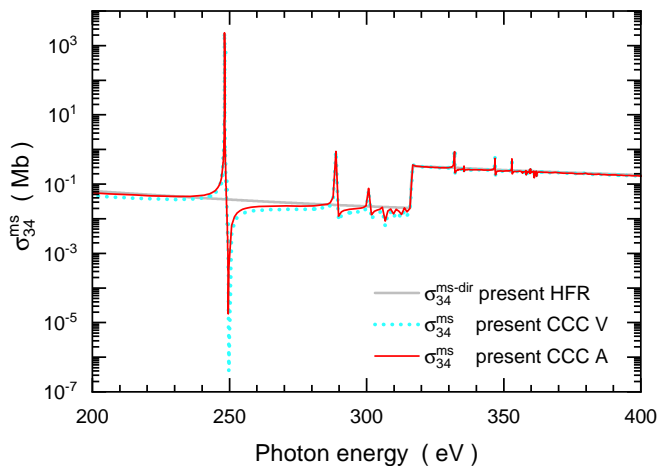


FIG. 6. (color online) Cross sections for net single photoionization of metastable $B^{3+}(1s2s^3S)$ ions. The solid red line and the dotted cyan line represent the cross section σ_{34}^{ms} obtained by CCC calculations in the acceleration and velocity gauges, respectively. The thick solid light-gray line is the direct-ionization cross section resulting from the present HFR calculations.

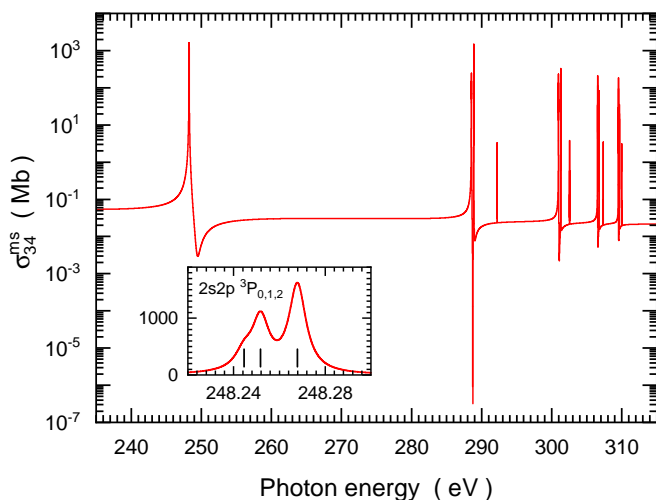


FIG. 7. Cross section for single photoionization of metastable $B^{3+}(1s2s^3S)$ ions obtained by MBPT calculations including the 40 energetically lowest 3P resonance levels. The inset shows the first resonance feature in the spectrum on a linear scale. The vertical bars indicate the calculated resonance energies from Table III.

K -shell excitation and reaches into the Gb range. This latter finding is confirmed by the MBPT approach.

The MBPT calculations were restricted to the 40 lowest-energy resonances in the photoionization cross section σ_{34}^{ms} . The results for the metastable $B^{3+}(1s2s^3S)$ ion are shown in Fig. 7. Different from Figs. 3, 6, and 7 where data are shown on a logarithmic cross-section scale, the inset of Fig. 7 displays the first resonance group on a linear scale. The associated resonance energies obtained by the present MBPT calculations are indicated

by the vertical bars. Due to the natural widths of the individual levels within the 3P term, the triplet structure of the resonance feature cannot fully be resolved even with infinite resolving power.

The resonance energies were determined with very high accuracy with uncertainties of less than ± 1 meV for most of the investigated resonance levels. Other parameters were obtained with estimated uncertainties of less than 1%. The calculated resonance parameters are provided in Table III. The cross section shown in Fig. 7 was evaluated from these parameters with the resulting resonance profiles added to the calculated cross section for direct ionization of metastable $B^{3+}(1s2s^3S)$.

As Table III shows, the maximum life-time widths of the investigated $^3P_{0,1,2}$ resonances are only slightly above 9 meV. In contrast, life-time widths of the 1P_1 resonances populated by double- K -shell excitation reach up to about 84 meV. In principle, the triplet P levels addressed by Table III can also be populated from the ground state. However, in that case, they require inter-combination transitions and, hence, are characterized by small resonance strengths. The level-specific parameters, i.e., the natural widths Γ , the Auger and radiative decay rates A_a and A_r , respectively, and the branching ratios of the 3P_1 levels for autoionization in the two tables are identical while the resonance energies, the resonance strengths S_{ion} , and the Fano parameters q are different since the transitions to the identical final levels start from different initial states.

It is interesting to compare the present resonance energies with the results of other calculations and with experimental data. The first observation of doubly excited heliumlike B^{3+} was reported by Kennedy and Carroll [90]. They found a wavelength of 49.934(5) Å for the transition $2s2p^3P \rightarrow 1s2s^3S$ without resolving the fine structure of the 3P term. The measured wavelength corresponds to a transition energy of 248.296(25) eV which is much closer to the present energy than most of the existing theoretical values. There are quite many calculations on doubly excited levels of He-like ions in the literature. Comparisons of a number of previous results for resonance energies and resonance widths of He-like atoms and ions with atomic numbers between 2 and 10 have been provided by Gning *et al.* [91]. The theoretical data for resonance energies show relatively large differences. For the $2\ell 2\ell'$ terms in the B^{3+} ion, they scatter around their mean with a standard deviation of more than 500 meV reaching maximum deviations of more than 2 eV. For the same resonances the previously calculated total widths deviate from one another by up to 26%.

A closer inspection shows that hardly any of the previous calculations match the high quality standards of the present theoretical work and, particularly, the present MBPT approach which is both relativistic and considers the most important quantum electrodynamic (QED) corrections. Only one theory publication on doubly excited states of B^{3+} could be found that claims a level of accuracy sufficient to challenge the results of the present work.

TABLE III. Calculated parameters (using MBPT) of the 40 lowest-energy resonance contributions to single photoionization of metastable $B^{3+}(1s2s^3S)$. With the exception of the $2s2p^1P_1$ level, the excited states are associated with 3P terms due to the selection rules for electric-dipole transitions. The first column provides the resonance level. Further entries are the resonance energies E_{res} (with converged partial-wave contributions) relative to the parent-ion initial state, the same energies without resonance QED corrections (and in the case of the $2s2p^1P$ resonance also without the 1.2 meV extrapolation correction) E_{res^*} , the natural (life-time) widths Γ , the Fano q parameters [81], the Auger decay rates A_a , the total radiative rates A_r , the branching ratios for Auger decay B_a , and the ionization resonance strengths S_{ion} . Numbers in square brackets are powers of 10.

level	E_{res} eV	E_{res^*} eV	Γ eV	q	A_a s^{-1}	A_r s^{-1}	B_a	S_{ion} MbeV
$2s2p^3P_0$	248.2446	248.2430	9.272[-3]	-2.701[2]	1.376[13]	3.307[11]	9.7653[-1]	4.404[0]
$2s2p^3P_1$	248.2518	248.2501	9.151[-3]	-2.703[2]	1.357[13]	3.307[11]	9.7621[-1]	1.321[1]
$2s2p^3P_2$	248.2679	248.2662	9.045[-3]	-2.708[2]	1.341[13]	3.307[11]	9.7593[-1]	2.201[1]
$2s2p^1P_1$	254.5966	254.5962	8.442[-2]	-9.006[1]	1.279[14]	3.702[11]	9.9711[-1]	4.383[-5]
$2s3p^3P_0$	288.5296	288.5288	3.853[-3]	-1.082[2]	5.629[12]	2.253[11]	9.6151[-1]	2.639[-1]
$2s3p^3P_1$	288.5343	288.5334	3.810[-3]	-1.108[2]	5.566[12]	2.227[11]	9.6152[-1]	8.155[-1]
$2s3p^3P_2$	288.5441	288.5433	3.785[-3]	-1.161[2]	5.533[12]	2.176[11]	9.6216[-1]	1.440[0]
$2p3s^3P_0$	288.8600	288.8595	3.337[-4]	-2.742[3]	2.081[11]	2.990[11]	4.1037[-1]	1.899[-1]
$2p3s^3P_1$	288.8646	288.8641	3.207[-4]	-2.995[3]	1.855[11]	3.018[11]	3.8071[-1]	5.188[-1]
$2p3s^3P_2$	288.8739	288.8734	2.962[-4]	-3.630[3]	1.428[11]	3.073[11]	3.1720[-1]	6.930[-1]
$2p3d^3P_0$	292.2146	292.2143	2.098[-4]	1.981[4]	2.304[8]	3.185[11]	7.2293[-4]	7.616[-5]
$2p3d^3P_1$	292.2114	292.2111	2.103[-4]	1.988[4]	1.096[9]	3.184[11]	3.4318[-3]	1.089[-3]
$2p3d^3P_2$	292.2061	292.2058	2.096[-4]	1.981[4]	3.197[8]	3.181[11]	1.0041[-3]	5.360[-4]
$2s4p^3P_0$	300.9549	300.9541	1.617[-3]	-1.291[2]	2.251[12]	2.068[11]	9.1586[-1]	1.070[-1]
$2s4p^3P_1$	300.9591	300.9583	1.600[-3]	-1.314[2]	2.228[12]	2.033[11]	9.1637[-1]	3.306[-1]
$2s4p^3P_2$	300.9674	300.9665	1.590[-3]	-1.358[2]	2.220[12]	1.968[11]	9.1856[-1]	5.838[-1]
$2p4s^3P_0$	301.2983	301.2978	2.735[-4]	-9.044[2]	1.187[11]	2.967[11]	2.8576[-1]	3.932[-2]
$2p4s^3P_1$	301.3023	301.3018	2.686[-4]	-9.508[2]	1.075[11]	3.006[11]	2.6337[-1]	1.057[-1]
$2p4s^3P_2$	301.3104	301.3100	2.572[-4]	-1.065[3]	8.259[10]	3.082[11]	2.1133[-1]	1.334[-1]
$2p4d^3P_0$	302.5443	302.5439	1.980[-4]	-2.379[4]	2.421[8]	3.006[11]	8.0478[-4]	3.387[-5]
$2p4d^3P_1$	302.5415	302.5411	1.994[-4]	-2.186[4]	2.818[9]	3.002[11]	9.3000[-3]	1.185[-3]
$2p4d^3P_2$	302.5364	302.5360	1.972[-4]	-2.037[4]	2.417[8]	2.994[11]	8.0672[-4]	1.747[-4]
$2s5p^3P_0$	306.5362	306.5354	8.578[-4]	-1.338[2]	1.100[12]	2.037[11]	8.4367[-1]	4.818[-2]
$2s5p^3P_1$	306.5403	306.5394	8.502[-4]	-1.374[2]	1.094[12]	1.976[11]	8.4700[-1]	1.522[-1]
$2s5p^3P_2$	306.5477	306.5468	8.446[-4]	-1.441[2]	1.097[12]	1.864[11]	8.5477[-1]	2.794[-1]
$2p5s^3P_0$	306.7499	306.7495	2.418[-4]	-7.461[2]	7.213[10]	2.953[11]	1.9633[-1]	1.247[-2]
$2p5s^3P_1$	306.7537	306.7533	2.409[-4]	-8.002[2]	6.376[10]	3.023[11]	1.7417[-1]	3.153[-2]
$2p5s^3P_2$	306.7616	306.7612	2.342[-4]	-9.541[2]	3.981[10]	3.160[11]	1.1191[-1]	3.025[-2]
$2p5d^3P_0$	307.3603	307.3599	1.940[-4]	-2.225[4]	3.077[7]	2.948[11]	1.0437[-4]	2.121[-6]
$2p5d^3P_1$	307.3577	307.3572	1.974[-4]	-1.771[4]	5.185[9]	2.948[11]	1.7285[-2]	1.072[-3]
$2p5d^3P_2$	307.3527	307.3523	1.924[-4]	-1.538[4]	6.085[7]	2.923[11]	2.0810[-4]	2.231[-5]
$2s6p^3P_0$	309.5020	309.5012	5.380[-4]	-1.354[2]	6.152[11]	2.022[11]	7.5260[-1]	2.381[-2]
$2s6p^3P_1$	309.5061	309.5053	5.326[-4]	-1.412[2]	6.182[11]	1.910[11]	7.6391[-1]	7.830[-2]
$2s6p^3P_2$	309.5129	309.5120	5.248[-4]	-1.512[2]	6.234[11]	1.739[11]	7.8185[-1]	1.526[-1]
$2p6s^3P_0$	309.6371	309.6367	2.220[-4]	-6.758[2]	4.761[10]	2.898[11]	1.4111[-1]	5.051[-3]
$2p6s^3P_1$	309.6408	309.6404	2.245[-4]	-7.454[2]	4.291[10]	2.982[11]	1.2579[-1]	1.240[-2]
$2p6s^3P_2$	309.6488	309.6485	2.245[-4]	-9.972[2]	1.792[10]	3.232[11]	5.2523[-2]	7.126[-3]
$2p6d^3P_0$	309.9857	309.9853	1.935[-4]	6.530[4]	5.552[7]	2.940[11]	1.8881[-4]	2.056[-6]
$2p6d^3P_1$	309.9832	309.9827	1.936[-4]	-1.029[5]	8.317[9]	2.858[11]	2.8276[-2]	9.497[-4]
$2p6d^3P_2$	309.9784	309.9780	1.896[-4]	-4.056[4]	1.034[8]	2.879[11]	3.5904[-4]	2.135[-5]

TABLE IV. Comparison of parameters of $^{11}\text{B}^{3+}(2\ell 2\ell')$ resonances in single photoionization of metastable $\text{B}^{3+}(1s2s\ ^3S)$ and ground-state $\text{B}^{3+}(1s^2\ ^1S)$ originating from two different theoretical endeavors. Columns 2-5 provide the total binding energies for the doubly excited states resulting from the present MBPT approach, as well as those obtained by Zaytsev *et al.* [18]. In both cases the results after inclusion of the Coulomb and Breit interactions to all orders (DCB: Dirac-Coulomb-Breit) are given separately, and then the final results when recoil and QED effects are considered follow (see text for explanations). Columns 6-9 give the transition energies (Trans. en.) relative to the metastable $\text{B}^{3+}(1s2s\ ^3S)$ and the ground-state $\text{B}^{3+}(1s^2\ ^1S)$, using the results from Yerokhin *et al.* [55, 64]. Columns 10 and 11 present Auger widths Γ_A .

Reso- nance level	DCB energy		Total energy		Trans. en. from $1s2s\ ^3S$		Trans. en. from $1s^2\ ^1S$		Γ_A	
	present eV	Ref. [18] eV	present eV	Ref. [18] eV	present eV	Ref. [18] eV	present eV	Ref. [18] eV	present eV	Ref. [18] eV
$2s2p\ ^3P_0$	-152.79682	-152.79682	-152.7876	-152.7877	248.2446	248.2445			9.05[-3]	9.02[-3]
$2s2p\ ^3P_1$	-152.78968	-152.78968	-152.7804	-152.7806	248.2518	248.2516	446.8200	446.8199	8.93[-3]	8.92[-3]
$2s2p\ ^3P_2$	-152.77364	-152.77364	-152.7644	-152.7645	248.2679	248.2677			8.83[-3]	8.82[-3]
$2s2p\ ^1P_1$	-146.44455(10) ^a	-146.44445	-146.4356	-146.4358	254.5966	254.5964	453.1648	453.1646	8.42[-2]	8.41[-2]

^a The result with $\ell_{\max} = 10$ is -146.44334 eV, extrapolation from there gives the quoted result.

Zaytsev *et al.* [18] published high-accuracy energies and Auger widths for all the 10 levels possible in $2\ell 2\ell'$ doubly excited configurations of heliumlike ions with atomic numbers $Z \geq 5$.

Like the present calculation, Ref. [18] uses complex rotation to be able to treat autoionizing states, and includes correlation due to both the Coulomb and the Breit interactions. The methods differ, though, concerning the implementations. Reference [18] uses a B-spline basis and a configuration-interaction approach, while the present MBPT calculation employs a finite-difference basis combined with a many-body perturbation expansion. Apart from numerical uncertainties these methods should, however, be equivalent for two-electron systems. Where possible, the results of Ref. [18] for the $^{11}\text{B}^{3+}$ ion are compared with the present data in Table IV.

Zaytsev *et al.* presented the total energies of the excited levels. In order to compare with the present results shown in Tables II and III it is necessary to determine the excitation energies relative to the initial levels $^{11}\text{B}^{3+}(1s^2\ ^1S_0)$ and $^{11}\text{B}^{3+}(1s2s\ ^3S_1)$, respectively, which are relevant in the present context. The total energies of those levels were taken or inferred from previous publications in which exceptionally small uncertainties are quoted. By extending calculations to include two-electron QED effects to all orders in the nuclear binding strength parameter $Z\alpha$, with the fine-structure constant α , Yerokhin *et al.* [55] were able to obtain the most accurate theoretical predictions to date for the ionization energies of the lowest levels of heliumlike ions with $Z = 5$ to $Z = 30$. Numbers for B^{3+} are provided in Table I. The determination of the total energy of the doubly excited levels requires the additional knowledge of the binding energy of the electron in H-like $^{11}\text{B}^{4+}(1s\ ^2S_{1/2})$. Yerokhin and Shabaev [64] provided ionization and excitation energies of $n = 1$ and $n = 2$ levels of hydrogenlike atoms and ions on the basis of *ab initio* QED calculations performed to all orders in the nuclear binding strength parameter $Z\alpha$ with Z ranging from 1 to 110. By com-

paring the information from the two cited papers, it is possible to infer very accurate total energies as well as ionization and excitation energies (see Table I) that can be employed for the comparison of the present findings with the data of Zaytsev *et al.*

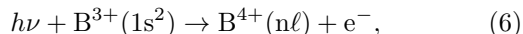
The results obtained with the present MBPT method and by the theoretical approach chosen by Zaytsev *et al.* [18] are in excellent agreement with one another. In fact the results on the Dirac-Coulomb-Breit (DCB) level [where the effects of the Coulomb and Breit interactions are fully accounted for but no effects due to the quantization of the electromagnetic field (QED effects for short) are considered yet] agree to all quoted digits for the triplet levels. Here, the summation over partial waves is converged and no extrapolation is needed. The partial-wave convergence is much slower for the $2s2p\ ^1P_1$ state and here we find that contributions from $\ell \geq 11$ change the results by about 1.2 meV. With this contribution added, the present results agree to within a few tenths of a meV with (the also extrapolated) values from Ref. [18] where the authors calculated QED and recoil effects from first principles. Here, we only add the reduced-mass effect and estimate the QED effects as explained in Sec. III A. Still our results agree to within 0.2 meV with that from Ref. [18] as detailed in Table IV. This gives confidence in our values for the resonances $2\ell n\ell'$ with $n > 2$, where no first-principle calculations of QED and recoil effects are available.

The differences of the calculated Auger widths Γ_A obtained by the two theoretical approaches are remarkably small. They are only 0.01 meV with one exception, the width of the $2s2p\ ^3P_0$ resonance, where the result of the present calculation is 0.03 meV above that of Zaytsev *et al.* The uncertainties of the latter results were quoted to be between 0.01 and 0.02 meV, thus essentially explaining the small differences. As mentioned above, calculated widths in previous publications differ from one another by up to 26%. The differences between the present results and the calculations of Zaytsev *et al.* are less than 0.3%.

Obviously, a milestone of accuracy has been reached in the present theoretical approach as well as in the St. Petersburg group's methodology in calculating resonance parameters for doubly excited states of two-electron systems.

C. Contributions of ionization-excitations to net single photoionization of B^{3+}

Beside direct photoionization and indirect ionization processes involving the excitation of autoionizing levels in the parent ion and subsequent Auger decay, there is a third mechanism, IE, by which the parent ion finally ends up in the channel of net single ionization. In such processes, one of the electrons in the parent A^{q+} ion is directly removed by a single photon while a second electron is lifted to an excited state of the $A^{(q+1)+}$ ion. In a He-like ion such as ground-state B^{3+} , the IE mechanism can be described as



with the B^{4+} ion in an excited state with principal quantum number $n \geq 2$ and orbital quantum number ℓ . The CCC calculations reported here for single photoionization comprise all three net ionization channels discussed so far. In addition, CCC also addresses indirect processes that produce excited $B^{4+}(n\ell)$ levels. Such indirect processes may involve, for example, the population of intermediate doubly excited resonances such as $B^{3+}(3pnd)$ that can decay to $B^{4+}(2s) + e^-$ provided that $n \geq 3$.

By the present CCC calculations, cross sections σ_{34IE}^{gs-n} were obtained for IE processes described by Eq. 6 for the ground state of B^{3+} without specifying the orbital quantum number ℓ , that is, the cross sections are summed over all possible ℓ for each n . The principal quantum numbers n range from $n = 2$ to $n = 6$. Similar calculations have been published previously for photoionization of the helium isoelectronic sequence [67]. In the present new calculations, the density of energy steps was increased relative to the calculations in Ref. [67] to see the effects of resonance contributions. Figure 8 shows the cross sections σ_{34IE}^{gs-n} for different final principal quantum numbers n as a function of the photon energy. Clearly, the threshold for producing B^{4+} increases with n . According to the calculations by Yerokhin *et al.* [55, 64] the energy required to produce $B^{4+}(2s)$ is 514.53533 eV (see Table I). This is approximately the onset of the calculated cross section σ_{34IE}^{gs-2} . The onsets of the partial cross sections increase according to the excitation energies of hydrogenlike $B^{4+}(n\ell)$.

The first resonance in the cross section σ_{34IE}^{gs-2} at an energy of approximately 532 eV with its pronounced Fano profile is associated with intermediate $B^{3+}(3s3p^1P)$ autoionizing to $B^{4+}(n=2) + e^-$. Higher-lying resonances can be identified on the basis of the assignments provided in Fig. 4. It is interesting to see the relatively

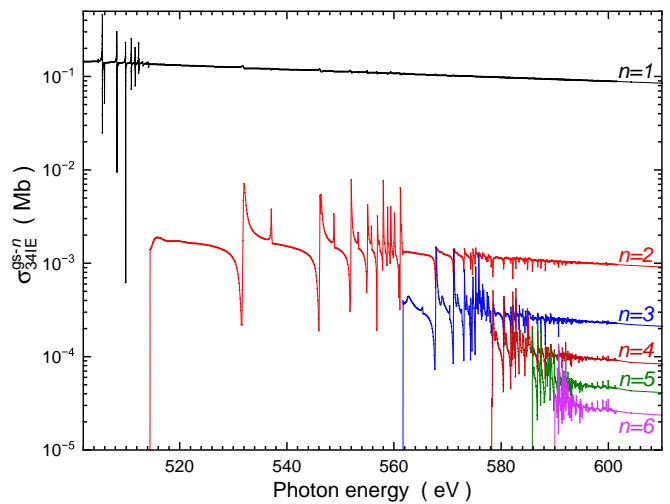


FIG. 8. (color online) Cross sections σ_{34IE}^{gs-n} for IE of $B^{3+}(1s^2 \ ^1S)$ with production of $B^{4+}(n)$ where the remaining electron is found in shell n with $n = 2, 3, \dots, 6$. For comparison, the cross section for single ionization without excitation (the black curve labeled $n = 1$) is also shown. The data were obtained by the present CCC calculations.

large resonance contributions to the IE cross sections for excitations to higher principal quantum numbers n . When n increases the continuum cross section for direct IE strongly decreases (approximately with n^{-3} for $n \geq 2$ with the scaling getting better for higher n) so that the resonances riding on that continuum clearly stick out.

Especially important in the present context is the size of the IE cross sections. They are all well below 10^{-2} Mb and they rapidly drop with increasing n . The present CCC calculations also yielded σ_{34IE}^{gs-1} which is the sum of the cross sections σ_{34}^{gs-dir} for direct single photoionization of the B^{3+} ground-state ion and the associated resonance contributions or, in other words, the cross section for net single ionization of $B^{3+}(1s^2 \ ^1S)$ producing ground-level $B^{4+}(1s)$ without any excitation. Thus, obviously, σ_{34IE}^{gs-1} does not contribute to the total IE cross section. The label ‘‘IE’’ just characterizes the partial, no-excitation cross section with $n = 1$ from the series σ_{34IE}^{gs-n} .

The CCC calculations show that σ_{34IE}^{gs-1} is almost as large as σ_{34}^{gs} , the cross section for net single ionization of B^{3+} (shown in Fig. 3). The difference of the latter two cross sections is the total cross section σ_{34IE}^{gs} for IE of ground-state B^{3+} , i.e., for the process described by Eq. 6 summed over all $n \geq 2$

$$\sigma_{34IE}^{gs} = \sigma_{34}^{gs} - \sigma_{34IE}^{gs-1} \quad (7)$$

which is approximately only of the order of 1.5% to 2% of σ_{34}^{gs} and can, therefore, be neglected in the present investigation of single photoionization of ground-level B^{3+} .

IE calculations were also performed for the metastable levels $1s2s \ ^1,3S$ of the B^{3+} ion. The results are similar to those for the ground-state ion in that the contributions of IE are also negligible relative to net single ionization

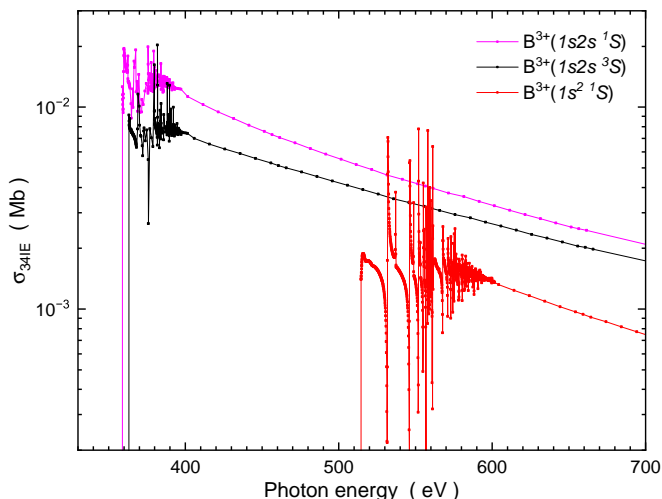


FIG. 9. (color online) Total cross sections σ_{34IE} for IE of $B^{3+}(1s^2 \ ^1S)$, $B^{3+}(1s2s \ ^1S)$, and $B^{3+}(1s2s \ ^3S)$ ions. The lowest excitation function (red) belongs to the initial B^{3+} ion in its ground state. The next above that (black) belongs to the initial ion in the $1s2s \ ^3S$ level. The largest IE cross section is found for the $1s2s \ ^1S$ level. The small square dots are the cross sections obtained from CCC calculations. They are connected by straight colored lines to highlight the energy dependence of the cross sections.

of B^{3+} . The population of $B^{4+}(n)$ states with $n = 1$ and $n = 2$ is almost exclusively due to direct removal of the $2s$ electron or the $1s$ electron, respectively. At the threshold of K -shell ionization the contribution of direct removal of the $2s$ electron is only about 4% of σ_{34}^{ms} for the initial $1s2s \ ^3S$ level and about 6.7% for the initial $1s2s \ ^1S$ level.

Figure 9 shows the initial-level-dependent total cross sections σ_{34IE} for IE of $B^{3+}(1s^2 \ ^1S)$, $B^{3+}(1s2s \ ^1S)$, and $B^{3+}(1s2s \ ^3S)$ ions obtained from the CCC calculations. The total IE cross sections are determined by summing the partial IE cross sections over the principal quantum numbers n of the final levels. For the ground state the summation starts at $n = 2$, for the metastable levels it starts at $n = 3$. In reality, the infinite sums are obtained by following the recipe of Eq. 7, i.e., by subtracting the contributions of single ionization without excitation from the net single ionization cross sections obtained by CCC calculations.

In the case of ground-state B^{3+} the total IE cross section σ_{34IE}^{gs} near its threshold oscillates around approximately 1.5 kb due to the effects of resonance contributions. The IE cross sections for the metastable levels are much larger at their considerably lower onsets, however, their relative contributions to the associated net single ionization are only of the order of a few percent. In conclusion, the contributions of ionization-excitation processes to the net single photoionization of B^{3+} are all relatively small and can be neglected in the present context. Consequently, the net single ionization cross sections can be described as the sum of the well understood smooth

direct-ionization continuum and the indirect, typically narrow, resonance contributions which reside on top of the smooth continuum cross section.

V. NORMALIZATION OF THE EXPERIMENTAL SINGLE-IONIZATION CROSS SECTION

The findings of the previous section, and particularly the uniformity of the results shown in Fig. 1, justify the normalization of the measured ion yields to the smooth total direct-ionization continuum of the net single-ionization cross section. Given the quality of the resonance parameters obtained from the MBPT calculations, it is also possible to determine the fraction f of metastable $1s2s \ ^3S$ ions in the parent B^{3+} beam. For this purpose, a scan of the photon-energy region 288.24 to 288.95 eV was analyzed. In this energy range, the contributions of three partial cross sections are responsible for the measured yield Y of B^{4+} photoionization products. The processes that can happen are (i) the direct ionization of the $2s$ subshell of metastable B^{3+} ions in the parent-ion beam, (ii) the direct ionization of the K shell of ground-state B^{3+} parent ions, and (iii) the resonant K -shell excitation and subsequent autoionization of the metastable B^{3+} parent ions. No K -shell direct ionization of metastable ions is possible in the chosen energy range as manifested by Table I. Consequently, IE even only involving the minimum excitation to $B^{4+}(2p_{3/2})$ with its threshold at 315.9938 eV (see Table I) is also energetically forbidden and could be neglected anyway. Hence, the apparent cross section behind the experimental B^{4+} yield Y in Fig. 10 can be represented as

$$\sigma_{34}^{app} = (1 - f)\sigma_{34}^{gs-dir} + f\sigma_{34}^{ms-dir} + f\sigma_{34}^{ms-res} \quad (8)$$

where the resonance contribution σ_{34}^{ms-res} resulting from K -shell excitation of metastable B^{3+} is derived from the data provided in Table III. From the measured resonance energies one may conclude that the two peak features are due to the $2s3p \ ^3P_{0,1,2}$ and $2p3s \ ^3P_{0,1,2}$ intermediate doubly excited states. Compared to the data in Table III the measured resonances are slightly shifted by about 0.1 eV towards lower energy. The experimental energy scale has to be corrected accordingly. The smooth continuum is related to the cross sections σ_{34}^{gs-dir} and σ_{34}^{ms-dir} from Figs. 1 and 2, respectively. A somewhat arbitrary representation of the ground-state direct ionization was chosen as the arithmetic mean of the results obtained by Verner *et al.* [78] and by Mikhailov *et al.* [79]. It falls right into the narrow span of theoretical cross-section data displayed in Fig. 1. At 288.6 eV this cross section is $\sigma_{34}^{gs-dir} = 0.558$ Mb while $\sigma_{34}^{ms-dir} = 0.025$ Mb according to the present HFR calculations.

Based on Fig. 1, an estimate of the relative uncertainty of the chosen model cross section for direct K -shell single ionization is $\pm 10\%$. At 288.6 eV this amounts to a possible error of 0.056 Mb. With the available data

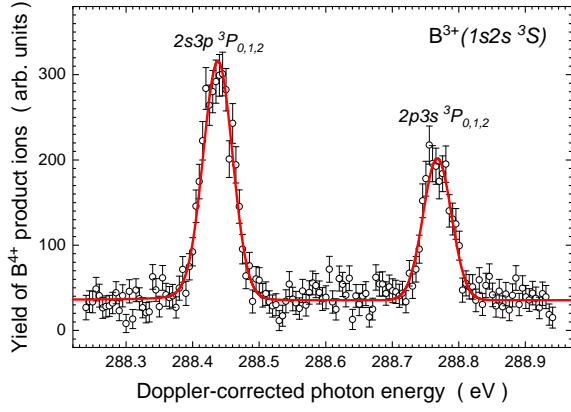


FIG. 10. (color online) Measured B^{4+} product-ion yield in the photon-energy range where $2s3p\ ^3P$ and $2p3s\ ^3P$ resonances are found to arise from single K -shell excitation of metastable $B^{3+}(1s2s\ ^3S)$. The data were taken with a $200\ \mu\text{m}$ monochromator exit-slit size. The yields are provided in arbitrary units. The solid red line is a fit to the measured yield based on the results of MBPT theory. An energy resolution of $48(2)\ \text{meV}$ was found by the fit.

base being much smaller for the metastable ions, a more conservative estimate of $\pm 20\%$ is taken into account for the cross section $\sigma_{34}^{\text{ms-dir}}$. From previous experiments a metastable fraction f close to 0.1 has to be expected implying that the smooth continuum cross section behind the yield Y shown in Fig. 10 is given approximately by $(0.9 \times 0.558 + 0.1 \times 0.025)\ \text{Mb} \approx 0.9 \times 0.561\ \text{Mb}$. The contribution of direct ionization of the $2s$ subshell of metastable $B^{3+}(1s2s\ ^3S)$ is less than 0.6% of the cross section $\sigma_{34}^{\text{gs-dir}}$ and can, therefore, be expected to have little effect in Eq. 8.

The calculated strengths of the 6 resonance levels contributing to the yield curve in Fig. 10 can be taken from Table III. In total, they amount to $S^{\text{theo}} = 3.921\ \text{Mb eV}$. The experimental resonance strength S^{exp} can be derived from a fit to the experimental B^{4+} yield Y in Fig. 10. The fit shown in the figure by a solid red line was performed by keeping the theoretical resonance energies E_{res} , natural widths Γ , Fano parameters q , and ionization strengths S_{ion} constant while the photon-energy bandwidth w_G , an energy shift ΔE_{ph} , a scale factor $A = S^{\text{exp}}/S^{\text{theo}}$, and a constant background B were used as fit parameters. The fitted curve matches the experimental data very well as evidenced by Fig. 10.

An energy shift $\Delta E_{\text{ph}} = 0.1012(7)\ \text{eV}$ was found. It represents the photon-energy calibration error of the beamline in the vicinity of $E_{\text{ph}} = 290\ \text{eV}$ at the time of the specific measurement. This error was corrected for in the subsequent analysis. The energy resolution was found to be $w_G = 48.2(1.7)\ \text{meV}$ for the measurement shown in Fig. 10 which was not sufficient to resolve the fine structure of the two resonance terms. The background $B = 35.59(1.40)\ \text{y.u.}$ (yield units) corresponds to the experimental yield Y outside of the resonances, i.e.,

the contribution of non-resonant direct ionization. The scale factor came out to be $A = 6.35(19)\ \text{y.u. Mb}^{-1}$. Introducing the factor N for normalizing a measured yield to the absolute cross-section scale leads to a set of simple equations linking the fit parameters A and B to the experimental and theoretical data

$$NB = (1-f)\sigma_{34}^{\text{gs-dir}} + f\sigma_{34}^{\text{ms-dir}}, \quad (9)$$

$$NS^{\text{exp}} = fS^{\text{theo}}, \quad (10)$$

$$A = S^{\text{exp}}/S^{\text{theo}}. \quad (11)$$

By dividing the two first equations by one another, the normalization factor drops out and the parameter f can be determined from the numbers given in the text above. The resulting fraction of metastable ions is $f = 0.091$ and the normalization factor $N = 0.0143\ \text{Mb (y.u.)}^{-1}$. The error propagation gives $\Delta f = 0.016$ which corresponds to a relative uncertainty $\Delta f/f \approx 0.18$. This result, $f = 0.091(16)$, is fully compatible with the findings of a previous experiment [53] that suggested $f = 0.105$ (see the discussion in Sec. II).

The normalization factor N relating the measured yield and the absolute cross section depends on the photon energy E_{ph} . This energy dependence is mainly caused by changes of the shape of the photon beam while E_{ph} is scanned over a wide energy range. As a result, the beam overlap, the so-called form factor [48], may change with E_{ph} . Since that factor could not be measured during the present experimental campaign, the experimental yields were normalized to the theory for direct single ionization. In a long scan covering E_{ph} from about 250 to 1200 eV, the yield of B^{4+} ions produced by photoionization of a mixed beam of B^{3+} ions in the ground state and in the 3S metastable state was measured in steps of 5 eV. The photon-energy resolution for that scan was chosen by setting the monochromator exit-slit width to $1000\ \mu\text{m}$. At $E_{\text{ph}} \approx 450\ \text{eV}$ a resolution of 0.6 eV resulted from these settings. With the step width of 5 eV it is very unlikely to see evidence for resonance contributions to the measured yields and, indeed, the yield curve shows a smooth behavior.

The experimental yields are expected to follow the apparent cross section for a mixed B^{3+} ion beam with a fraction $1-f = 0.909$, i.e., 90.9%, of $1s^2\ ^1S$ ground-state ions and a fraction $f = 0.091$, i.e., 9.1% of metastable $1s2s\ ^3S$ ions. Without considering the resonance contributions, Eq. 8 takes the general form

$$\sigma_{34}^{\text{app}} = 0.909\sigma_{34}^{\text{gs-dir}} + 0.091(\sigma_{34}^{\text{ms-dir-1s}} + \sigma_{34}^{\text{ms-dir-2s}}) \quad (12)$$

where the partial cross sections for direct ionization of the metastable component by removal of the $1s$ or the $2s$ electron, respectively, are considered. By a smooth function $N(E_{\text{ph}})$ the experimental yield curve is adjusted to σ_{34}^{app} given by Eq. 12.

The resulting experimental apparent cross section is shown in Fig. 11. Obviously, the smooth normalization function $N(E_{\text{ph}})$ works well. The normalization devel-

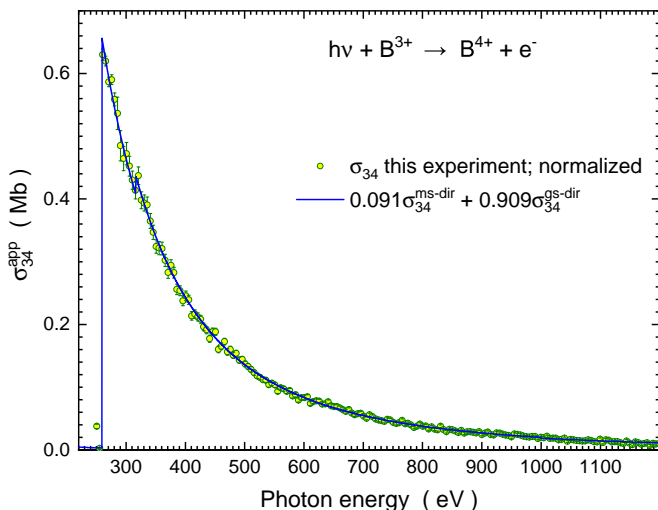


FIG. 11. (color online) Apparent experimental photoionization cross sections (yellow-shaded circles) normalized to the theoretical cross section (solid blue line) described in Eq. 12.

oped for the cross-section overview was then also employed to obtain the detailed cross-section results that deal with double- K -hole resonances.

VI. COMPARISON OF THEORY AND EXPERIMENT

The overview scan displayed in Fig. 11 with photon-energy steps of 5 eV did not show any signs of resonance structures in the apparent cross section σ_{34}^{app} . Such structures could only be revealed in measurements with step sizes smaller than 0.2 eV. After exploring the approximate positions of resonances with the monochromator exit slit wide open, dedicated measurements with increased resolution and smaller photon-energy steps were performed. The results of these measurements for metastable $B^{3+}(1s2s\ ^3S)$ and ground-state $B^{3+}(1s^2\ ^1S)$ are separately discussed in the following two subsections.

A. $B^{3+}(1s2s\ ^3S)$

The metastable $B^{3+}(1s2s\ ^3S)$ ions with their high excitation energy of 198.568 eV [55] already carry a K vacancy. A single K -shell excitation produces a doubly excited autoionizing level with two K holes, i.e., an empty K shell. The cross sections for such single excitations are relatively large but drop with increasing excitation energies. Resonance contributions with single K -shell excitations of metastable B^{3+} are to be expected in the energy range between the lowest-energy excitation to the $2s2p\ ^3P_{0,1,2}$ levels at about 248.245 eV and the K edge at 315.97 eV. These numbers are obtained by combining results of previous theoretical work [18, 55, 64]. See also

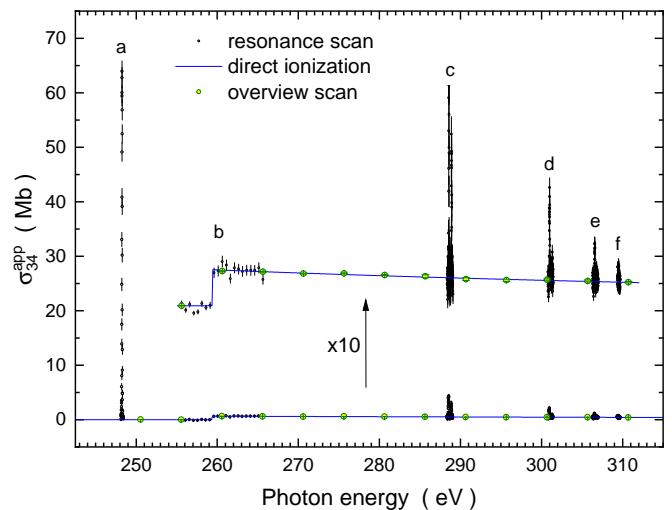


FIG. 12. (color online) Apparent experimental B^{3+} photoionization cross section normalized to the theoretical cross section (solid blue line) described in Eq. 12. The parent-ion beam consisted of a fraction of 90.9% of ground-state and 9.1% of metastable ions. The part of the spectrum shown with an offset was multiplied by a factor 10 for better visibility of the details. The small letters stand for characteristic cross-section features. The step b is the K edge of ground-state B^{3+} . The other features are highlighted in the subsequent two figures. The resonances are associated with $1s2s\ ^3S \rightarrow 2lnl'\ ^3P$ transitions with $\ell = s, p, n = 2, \dots, 6$, and $\ell' = p, s$, respectively.

Table I. At energies beyond the K edge, double excitations of both electrons in the $1s2s$ parent configuration can contribute to σ_{34}^{app} . However, the sizes of the associated resonances are small as the present CCC calculations suggest (see Fig. 6). Moreover, the contributions of these resonances to the experimental cross section σ_{34}^{app} are weighted by the fraction f of metastable ions in the parent-ion beam which strongly reduces their product ion yield while the continuum of direct ionization remains high. Therefore, the detection of these resonances was not attempted.

Figure 12 shows the experimental results of a set of B^{3+} resonance scans at moderate energy resolution obtained with a 200 μm exit-slit width of the monochromator. Photon-energy bandwidths were between approximately 37 and 55 meV, increasing with the resonance energy. Step sizes of 5 meV were chosen to scan the $1s2s\ ^3S \rightarrow 2lnl'\ ^3P$ resonances while the region of the $1s^2\ ^1S \rightarrow 1s\ ^2S + e^-$ ionization edge was covered with 0.5 eV steps. Along with the results of the fine resonance scans, the data of the overview scan of Fig. 11 that fall into the present energy range are also displayed. Their statistical uncertainties are relatively small because the signal rates at 1000 μm exit slit were considerably higher than those at 200 μm . Figure 12 also shows the apparent direct-ionization cross section described in Eq. 12. It is represented by the solid blue line. As mentioned

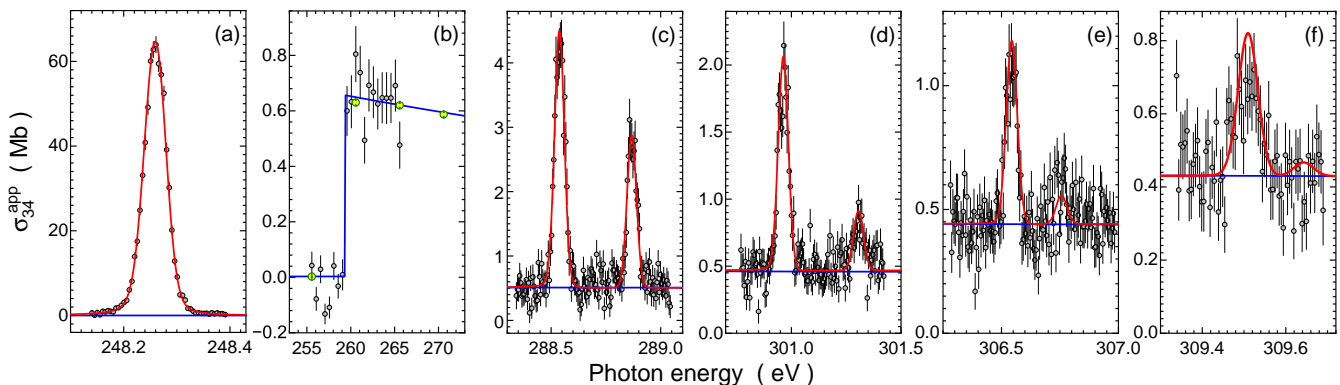


FIG. 13. (color online) Characteristic features in the apparent experimental photoionization cross sections for a mixed beam of B^{3+} ions. The labels of the individual panels correspond to the letters introduced in Fig. 12. The resonances are associated with K -shell excitation of metastable $1s2s\ ^3S$ ions, the threshold in panel (b) is the K edge of ground-state $1s^2\ ^1S$ ions. The solid blue line is the apparent direct ionization described by Eq. 12. The red lines show the results of the MBPT calculations for the resonance contributions (see Table III). The monochromator exit-slit width was $200\ \mu\text{m}$ which resulted in a resolving power $E/\Delta E \approx 6000$.

before, the photoion yields observed in the experiments were normalized to that cross section and thereby put on an absolute scale.

The letters a-f in Fig. 12 are associated with certain characteristic features in the photoionization of the mix of B^{3+} ions in the parent-ion beam. These features are shown separately in the six panels (a) - (f) of Fig. 13. While (b) stands for the K -shell ionization threshold of the ground-state component of the parent B^{3+} ion beam, the other letters represent resonances in the photoionization of metastable $B^{3+}(1s2s\ ^3S)$. They are associated with the 27 most strongly populated $^3P_{0,1,2}$ levels listed in Table III. With a resolving power around 6000, the fine structure of the 3P terms cannot be resolved. Thus, letter (a) represents the $B^{3+}(2s2p\ ^3P)$ term. Letter (c) comprises the 3P terms of configurations $2s3p$ and $2p3s$. Letter (d) stands for $2s4p$ and $2p4s$, (e) represents $2s5p$ and $2p5s$, and (f) comprises $2s6p$ and $2p6s$. The population of 1P levels is not strictly forbidden, however, intercombination transitions are strongly suppressed. The strongest such transition would have to be expected for the intermediate $2s2p\ ^1P$ level. The present MBPT calculations predict this level to have a resonance strength of 4.39×10^{-5} Mb eV in the photoionization channel - approximately 10^{-6} of the $2s2p\ ^3P$ strength and, therefore, too small to be seen in the present experiment at the expected resonance energy of 254.597 eV. The $2s2p\ ^1P$ resonance can, however, be populated from the ground state of B^{3+} without spin flip at a resonance energy of 453.165 eV (see Table II) and was clearly observed in the present experiments at higher photon energies (see below).

Table III additionally comprises the resonance parameters for 12 3P states based on configurations $2pnd$ with $n = 3, 4, 5, 6$. Although the transitions from the metastable 3S parent ion to these 12 levels are allowed in principle, their strengths are one to two orders of

magnitude smaller than the strengths of all other transitions mentioned in Table III. Accordingly, $2pnd$ resonances could not be observed experimentally. It should be mentioned that the configurations and spectroscopic level assignments used in the present paper only comprise the leading contributions in a multi-configuration representation.

The whole spectrum in Fig. 12 is dominated by the very strong $2s2p\ ^3P$ resonance term labeled a. The apparent cross section obtained with a mixed beam of ground-state and metastable B^{3+} at an energy resolution of 37 meV reaches a maximum of 65 Mb. Considering the fact, that only 9.1% of the parent-ion beam are responsible for the observed resonance a, the true cross section must have a maximum of more than 700 Mb. As Fig. 7 shows, the natural cross section (observable only at infinite resolving power) even reaches a maximum near 2 Gb.

Along with the experimental cross-section data, Fig. 13 shows the apparent direct-ionization cross section as a solid blue line that is already known from the preceding figures. In addition, the results of the MBPT calculations are displayed as solid red lines in the different panels (a), (c), (d), (e), and (f). The theoretical cross sections were convoluted [92] with Gaussian functions of increasing full width at half maximum (FWHM) to model the experimental energy spreads. Since the experimental results were obtained with a metastable ion-beam fraction of only 9.1% the theoretical cross sections were scaled down by a factor 0.091. The resulting red curves show a very good agreement with the experimental data.

The statistical quality of the experimental cross sections deteriorates with increasing excitation energy. The reason is in the decreasing cross sections and, hence, decreasing signal rates observed at increasing resonance energies. At the same time, the direct-ionization continuum becomes relatively more prominent as Fig. 13 clearly

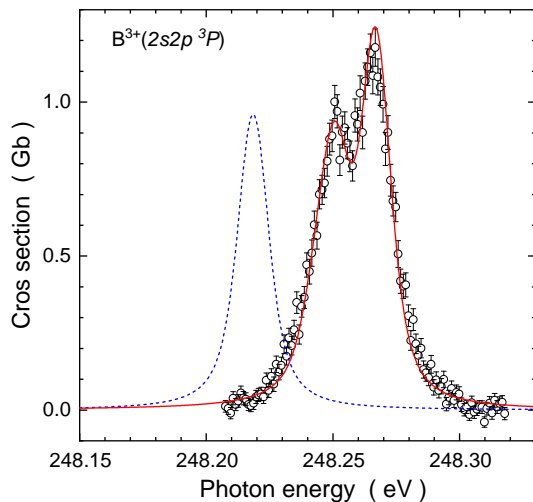


FIG. 14. (color online) High-resolution measurement of the $1s2s\ ^3S_1 \rightarrow 2s2p\ ^3P_{0,1,2}$ resonance contributions to the B^{3+} photoionization cross section normalized to represent the result for a pure ($f = 1$) metastable-ion ensemble. The data points were measured at an energy resolution of 8.5 meV. The solid red line is the cross section resulting from the MBPT calculations (see parameters in Table III). It was convoluted with a 8.5 meV FWHM Gaussian function to simulate the experimental energy resolution ($E/\Delta E \approx 29000$). The dashed blue line represents the (non-relativistic) CCC calculation convoluted and normalized accordingly, but multiplied by 0.5 so that the cross section size fits the diagram.

demonstrates and, therefore, isolating the resonant contribution to the apparent cross sections from that continuum becomes increasingly more difficult. We mention again that the experimental energy scale was calibrated to the theoretical resonance energies which are considered to be accurate within less than ± 1 meV.

The size of the $2s2p\ ^3P$ resonance allowed us to increase the resolving power of the experiment and still get measurable signal rates. By reducing the monochromator exit-slit width to 8 μm and by optimizing the fixed-focus constant c_{ff} [45, 93] of the variable-linespacing (VLS) grating in use at beamline P04, it was possible to carry out a measurement at a resolving power $E/\Delta E \approx 29000$. At the resulting photon-energy bandwidth of approximately 8.5 meV, the fine structure of the 3P term could be partially resolved. The result of this measurement is shown in Fig. 14. In this figure, the apparent experimental cross section was divided by a factor 0.091 in order to show the result for a parent-ion ensemble with a 100% fraction of metastable ions. Now the cross-section maximum reaches 1.2 Gb.

The solid red line in Fig. 14 is the theoretical MBPT cross section convoluted with a 8.5 meV FWHM Gaussian function modeling the experimental resolution. The shape of the experimental cross-section function agrees very well with the theoretical model. The figure also shows the cross section obtained from the present CCC

approach multiplied by a factor 0.5 and also convoluted with a 8.5 meV FWHM Gaussian function. It is represented by the dashed blue line. The CCC calculations are non-relativistic, i.e., the fine structure of the 3P term is not described. Therefore, the whole calculated strength is agglomerated in one single resonance while in reality, it is distributed over three fine-structure levels. Therefore, the CCC cross-section maximum is about a factor of two above the maximum of the MBPT result. In order to fit the CCC cross section on the same scale for display in Fig. 14, it was multiplied by the factor of 0.5.

The CCC calculations do not provide direct access to the resonance parameters. For each photon energy a separate calculation is necessary to obtain the cross section at that energy. In the present study an energy grid with a 10 meV spacing was chosen for the region close to the resonance energy. The wings of the $2s2p\ ^3P$ resonance were covered with an energy grid of 100 meV. The spacing of the resulting data points is sufficient for a meaningful fit of a Fano profile to these points. The following resonance parameters were obtained from the Fano fit to the CCC calculations: $E_{\text{res}} = 248.219$ eV, $\Gamma = 9.82$ meV, $q = -316$, and $S_{\text{ion}} = 39.645$ Mb eV. The resonance strength is practically identical with that obtained by MBPT for the 3P triplet (only 0.02 Mb eV less). The resonance energy is very slightly below (≈ 45 meV) the center of gravity of the MBPT calculation and the natural width Γ is a little greater (by less than 10%) than that obtained by the MBPT calculations for each of the 3P fine-structure components. The Fano parameter q is approximately 17% lower than that resulting from the MBPT calculations. All in all, there is a remarkable agreement of the CCC and MBPT results for the $2s2p\ ^3P$ resonance. However, at the level of a high experimental resolution such as the 8.5 meV accomplished in the present experiment, the relativistic MBPT calculations are clearly superior to the non-relativistic CCC calculations.

For the 3P resonances with higher excitation energies the step size of the CCC calculations is too large to facilitate meaningful fits of Fano resonance profiles so that a detailed comparison with the experiments or the MBPT calculations is not possible.

B. $B^{3+}(1s^2\ ^1S)$

The resonant ionization of ground-state $B^{3+}(1s^2\ ^1S)$ ions requires double K -shell excitation. Cross sections for such transitions by absorption of a single photon are relatively small as evidenced by the results of theoretical calculations shown in panels (a) and (b) of Fig. 3. The maxima of the double-excitation resonances are below 1 Mb which has to be compared with the ≈ 2 Gb $2s2p\ ^3P$ resonance that can be excited from the metastable $1s2s\ ^3S$ level. Accordingly, the resonances arising from the ground level are more difficult to detect in experiments. In the present measurements it was

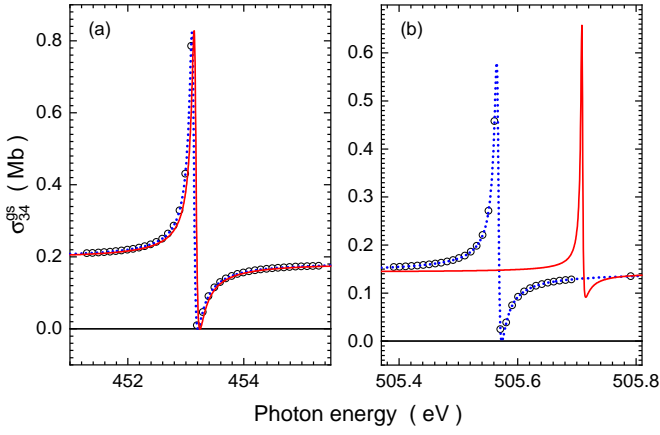


FIG. 17. (color online) Cross sections σ_{34}^{gs} for single photoionization of $\text{B}^{3+}(1s^2 \ ^1S)$ obtained by the present CCC and MBPT calculations. Panel (a) shows σ_{34}^{gs} in the vicinity of the $2s2p \ ^1P_1$ level and panel (b) the same in the region of the $2p5s/5d \ ^1P/3D$ resonance. The open circles are the results of CCC calculations at discrete photon energies. The dashed blue lines are Fano profiles fitted to the CCC data points. The solid red lines are the present MBPT results.

convoluted with a $w_G = 0.4$ eV FWHM Gaussian function and multiplied by a factor 0.909 (like the MBPT result). The short-dashed green line represents the smooth direct-ionization cross section obtained from the CCC calculation. At the present energy, this partial cross section is by far dominated by single K -shell ionization of ground-level B^{3+} . Therefore, the CCC result was also multiplied by a factor 0.909 to account for the fraction of ground-level ions in the parent B^{3+} ion beam. The short-dashed line agrees well with the present model for the direct-ionization contribution which is given by the smooth solid blue line. This supports the previous findings of very good agreement of theoretical direct-ionization cross sections (see Fig. 1). Both the CCC and MBPT cross sections σ_{34}^{app} are in excellent agreement with the experimental data as well as with one another.

The calculated CCC data points alone would not directly provide the level of agreement that is demonstrated in Fig. 16. As in the case of the $1s2s \ ^3S \rightarrow 2s2p \ ^3P$ transition, a Fano profile was first fitted to the calculated CCC data points. The individual data points and the fit function are shown in panel (a) of Fig. 17. Clearly, the calculated points with their somewhat arbitrarily chosen energies do not map out the full Fano profile. However, the density and precision of the calculated cross-section points facilitates the determination of the associated resonance parameters: the Fano fit curve delivers the resonance energy $E_{\text{res}} = 453.129$ eV (compared to 453.1648 eV from MBPT), the natural width $\Gamma = 0.087$ eV (compared to 0.08441 eV from MBPT), the Fano parameter $q = -1.818$ (compared to -1.833 from MBPT), and the ionization resonance strength $S_{\text{ion}} = 0.0602$ MbeV (compared to 0.05958 eV from MBPT).

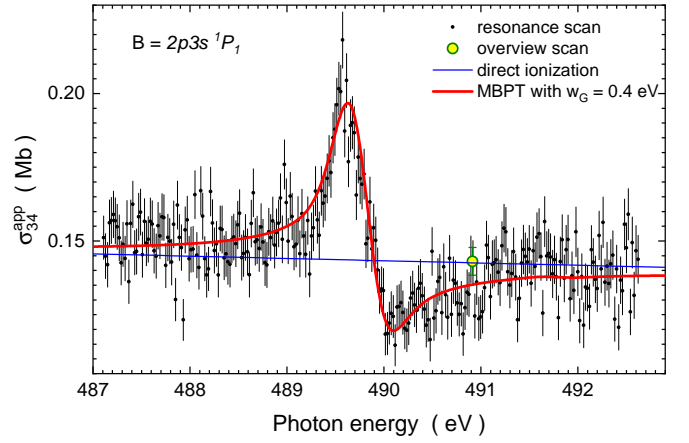


FIG. 18. (color online) Detail of Fig. 15 in the vicinity of peak feature B which corresponds to the $2p3s \ ^1P_1$ resonance.

The agreement of the calculated resonance energies obtained from CCC and MBPT is remarkably good but is fortuitous to some extent as the further analysis shows. The other parameters are in fair agreement with one another but show deviations that cannot be attributed to the uncertainties in the fitting procedure.

Panel (b) of Fig. 17 shows a second example of a direct comparison of CCC and MBPT calculations. In the particular case, the energy region around 505.5 eV is scrutinized where the $2p5s/5d \ ^1P/3D$ resonance gives the dominant contribution to σ_{34}^{gs} . As in panel (a), a Fano profile was fitted to the data points obtained by the CCC calculations at discrete photon energies. The resonance energy is about 0.15 eV different from that obtained by the MBPT calculations. The Fano q parameter derived from the fit is about 55% of the MBPT result and the lifetime width is a factor of 2 above that of the MBPT calculation. Only the resonance strengths S_{ion} from the two calculations agree within 25%. Given such discrepancies, no further comparisons of the experimental data and the resonance features seen in the CCC calculations at photon energies higher than 455 eV are presented.

Figure 18 zooms in on the $\text{B}^{3+}(2p3s \ ^1P)$ resonance observed in the experiment. The data shown are the same as in Fig. 15. The statistical uncertainties of the measured apparent cross sections indicate the increasing difficulty to isolate the resonant contributions from the direct-ionization continuum as the excitation energy increases. This is all the more true for further increasing principal quantum numbers $n = 4, 5, 6$ as evidenced by Fig. 19. No signal could be found for $n \geq 7$. In all cases, the experimental results confirm the theoretical results of the present MBPT calculations. Theoretical energies, total widths, shapes, and strengths of the doubly excited resonances fit the present experimental observations.

It is interesting to note that 28 resonances were predicted to occur in the present energy range from 444 to 518 eV but only 5 of them are sufficiently strong to be ob-

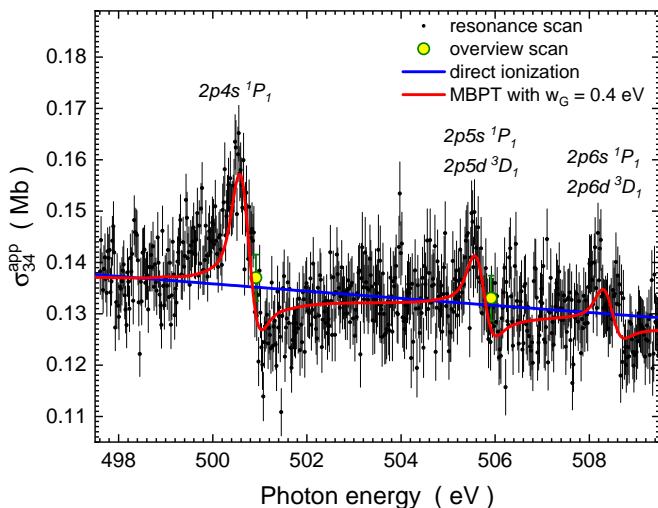


FIG. 19. (color online) Detail of Fig. 15 in the vicinity of peak features C, D, and E: the leading levels are indicated in the figure. The red line comprises all resonances calculated in the displayed energy range obtained by applying MBPT.

served in the experiments. The leading levels responsible for the labeled resonances in Fig. 15 are A = $2s2p\ ^1P$ at 453.1648 eV (see Table II), B = $2p3s\ ^1P$ at 489.7694 eV, C = $2p4s\ ^1P$ at 500.687 eV, D = $2p5s\ ^1P$ at 505.709 eV, and E = $2p6s\ ^1P$ at 508.426 eV. All the other resonances listed in Table II are blended with stronger resonance contributions or are too small to significantly contribute to the observed spectrum of double-excitation resonances which were all measured with a resolution of approximately 0.4 eV. Accordingly, the MBPT results shown in Figs. 15, 16, 18, and 19 were all convoluted with a 0.4 eV FWHM Gaussian function to simulate the experiment. They were also multiplied by a factor 0.909 to account for the 90.9% fraction of $1s^2$ ground-level B^{3+} ions that were present in the parent-ion beam.

VII. SUMMARY AND CONCLUSIONS

The present experimental and theoretical study investigates the role of double- K -hole resonances in the net single photoionization of heliumlike B^{3+} ions initially in their $1s^2\ ^1S_0$ ground level or initially in their $1s2s\ ^3S_1$ metastable excited level. The selection rules for electromagnetic transitions mediated by a single photon favor the production of $2lnl'\ ^1P_1$ doubly excited levels from ground-state ions and $2lnl'\ ^3P_{0,1,2}$ doubly excited levels from the metastable 3S excited parent ions. In the experiments, resonances in both, the singlet and triplet manifolds were observed with $n = 2, 3, 4, 5,$ and 6 . The experiments were accompanied by calculations employing the convergent close coupling (CCC) method and many-body perturbation theory (MBPT). Cross sections for direct single ionization of $1s$ and $2s$ electrons were calcu-

lated by employing relativistic Hartree-Fock (HFR) theory and the random-phase approximation with exchange (RPAE).

Direct single K -shell photoionization has been a topic of theoretical descriptions already since the early development of quantum mechanics. Comparison of altogether eight different approaches to direct single K -shell ionization of heliumlike B^{3+} shows that the results are very consistent with one another. In fact, they are identical within maximum deviations of $\pm 10\%$. This provides an accuracy for normalizing experimental yields of ionized ions that can hardly be matched by the conventional absolute measurement of cross sections in merged-beams experiments with photon and ion beams. By exploiting this observation, the present experimental B^{4+} product-ion yields were normalized to the smooth direct-ionization continuum on which the resonant contributions reside. For a meaningful normalization, the fractions $1 - f$ of ground-state and f of metastable B^{3+} ions in the parent-ion beam had to be quantified. This was accomplished by comparing measured yields of B^{4+} product ions with the results of the present MBPT calculations. A fraction $f = 0.091 \pm 0.016$ was found for the $1s2s\ ^3S$ component.

The MBPT results obtained in this study are of particularly high quality. Resonance energies are estimated to be correct within uncertainties of less than ± 1 meV for nearly all of the investigated levels. For the $2lnl'\ ^1P$ levels with $n \geq 4$ the uncertainties are slightly higher than that but still estimated to be lower than 2 meV. The high accuracy of these resonance energies makes the resonances in the single photoionization of B^{3+} ideal reference standards for calibrating the energies of photon beam lines as well as photon and (photo)electron spectrometers. The advantage of using He-like B^{3+} for calibration can be illustrated by comparing with one of the most commonly used energy reference standards, the neutral N_2 molecule, where resonance features around 400 eV are known with a quoted uncertainty of ± 20 meV [56] which is roughly a factor of 20 larger than what has been accomplished in the present work. Common reference standards for the next higher energies around 530 eV employ K -shell excitations in oxygen-containing molecules such as neutral CO and have uncertainties even as large as 60 to 90 meV [56]. Even the recent calibration work on Ne, CO_2 , and SF_6 employing the theoretical sub-meV uncertainties of level energies in heliumlike ions has resulted in uncertainties of 100 meV, 40 meV, and 60 meV, respectively, for the calibration-reference gases [57].

The huge cross section of the $1s2s\ ^3S_1 \rightarrow 2s2p\ ^3P_{0,1,2}$ resonance term with small natural widths (approximately 9 meV) of each fine-structure component provides particularly comfortable signal rates in energy-calibration measurements at about 248 eV. The calculated resonance parameters natural width Γ , Fano parameter q , and ionization strength S_{ion} are estimated to be correct within $\pm 1\%$. A comparison of Auger widths of the $2s2p\ ^{1,3}P$

levels obtained by the present MBPT calculations with results [18] obtained by the St. Petersburg theory group, that is renowned for highest-quality atomic-structure calculations, shows deviations of less than 0.3%. This is particularly remarkable since previous calculations of these Auger widths show a scatter of about 30%.

The present CCC calculations provided not only the cross sections for net single ionization of $B^{3+}(1s^2\ ^1S)$ and $B^{3+}(1s2s\ ^3S)$ but also yielded partial cross sections for single ionization accompanied by excitation of the remaining electron to different main shells with principal quantum numbers n up to 6. The sum of ionization-excitation contributions to the net single photoionization cross section σ_{34}^{gs} of heliumlike ground-state B^{3+} is only about 1.5% to 2%. The situation for metastable parent ions is similar.

The results obtained within the present investigation on photoionization of heliumlike B^{3+} are much more comprehensive than previous works on heliumlike $Li^+(1s^2\ ^1S)$ [43] and $C^{4+}(1s2s\ ^3S)$ [44].

Future work on photon interactions with heliumlike B^{3+} ions will address the removal of both electrons by direct single-photon double ionization.

VIII. ACKNOWLEDGEMENT

We acknowledge DESY (Hamburg, Germany), a member of the Helmholtz Association HGF, for the provision of experimental facilities. Parts of this research were carried out at beamline P04 of PETRA III. Beamtime was allocated for proposal I-20220764. We gratefully acknowledge support from Bundesministerium für Bildung und Forschung provided within the “Verbundforschung” funding scheme (Contracts No. 05K19GU3 and No. 05K19RG3). FT acknowledges funding by the Deutsche Forschungsgemeinschaft (DFG, German Research Foundation) - Project 509471550, Emmy Noether Programme. MM acknowledges funding of SFB925/A3 by Deutsche Forschungsgemeinschaft via Grant No. 2012673. Support from the Swedish Research Council (Grant No. 2020-03315) is gratefully acknowledged. ASK and IB acknowledge the support of the Australian Research Council, the National Computer Infrastructure, and the Pawsey Supercomputer Centre of Western Australia.

-
- [1] L. S. Cederbaum, F. Tarantelli, A. Sgamellotti, and J. Schirmer, On double vacancies in the core, *J. Chem. Phys.* **85**, 6513 (1986).
- [2] R. Santra, N. V. Kryzhevoi, and L. S. Cederbaum, X-ray two-photon photoelectron spectroscopy: A theoretical study of inner-shell spectra of the organic para-aminophenol molecule, *Phys. Rev. Lett.* **103**, 013002 (2009).
- [3] N. Berrah, L. Fang, B. Murphy, T. Osipov, K. Ueda, E. Kukk, R. Feifel, P. van der Meulen, P. Salen, H. T. Schmidt, R. D. Thomas, M. Larsson, R. Richter, K. C. Prince, J. D. Bozek, C. Bostedt, S. Wada, M. N. Piancastelli, M. Tashiro, and M. Ehara, Double-core-hole spectroscopy for chemical analysis with an intense x-ray femtosecond laser, *Proc. Natl. Acad. Sci. U.S.A* **108**, 16912 (2011).
- [4] M. Nakano, F. Penent, M. Tashiro, T. P. Grozdanov, M. Žitnik, S. Carniato, P. Selles, L. Andric, P. Lablanquie, J. Palaudoux, E. Shigemasa, H. Iwayama, Y. Hikosaka, K. Soejima, I. H. Suzuki, N. Kouchi, and K. Ito, Single photon K^{-2} and $K^{-1}K^{-1}$ double core ionization in C_2H_{2n} ($n = 1 - 3$), CO, and N_2 as a potential new tool for chemical analysis, *Phys. Rev. Lett.* **110**, 163001 (2013).
- [5] I. Ismail, A. Ferté, F. Penent, R. Guillemin, D. Peng, T. Marchenko, O. Travnikova, L. Inhester, R. Taïeb, A. Verma, N. Velasquez, E. Kukk, F. Trinter, D. Kouliantianos, T. Mazza, T. M. Baumann, D. E. Rivas, Y. Ovcharenko, R. Boll, S. Dold, A. De Fanis, M. Ilchen, M. Meyer, G. Goldsztejn, K. Li, G. Doumy, L. Young, G. Sansone, R. Dörner, M. N. Piancastelli, S. Carniato, J. D. Bozek, R. Püttner, and M. Simon, Alternative pathway to double-core-hole states, *Phys. Rev. Lett.* **131**, 253201 (2023).
- [6] F. Trinter, L. Inhester, R. Püttner, S. Malerz, S. Thürmer, T. Marchenko, M. N. Piancastelli, M. Simon, B. Winter, and U. Hergenbahn, Radiationless decay spectrum of O 1s double core holes in liquid water, *J. Chem. Phys.* **160**, 194503 (2024).
- [7] G. W. F. Drake, Theoretical energies for the $n=1$ and $n=2$ states of the helium isoelectronic sequence up to $Z=100$, *Can. J. Phys.* **66**, 586 (1988).
- [8] L. B. Madsen, Triply excited states: electron-electron correlations in lithium, *J. Phys. B: At. Mol. Opt. Phys.* **36**, R223 (2003).
- [9] P. Indelicato, QED tests with highly charged ions, *J. Phys. B: At. Mol. Opt. Phys.* **52**, 232001 (2019).
- [10] V. A. Zaytsev, A. V. Malyshev, and V. M. Shabaev, Complex-scaled ab initio QED approach to autoionizing states, *Phys. Rev. A* **107**, 032801 (2023).
- [11] R. P. Madden and K. Codling, New autoionizing atomic energy levels in He, Ne, and Ar, *Phys. Rev. Lett.* **10**, 516 (1963).
- [12] J. M. Rost, K. Schulz, M. Domke, and G. Kaindl, Resonance parameters of photo doubly excited helium, *J. Phys. B: At. Mol. Opt. Phys.* **30**, 4663 (1997).
- [13] F. J. Wuilleumier, From doubly excited states of helium to triply excited states of lithium, *Physics Essays* **13**, 230 (2000).
- [14] G. Tanner, K. Richter, and J.-M. Rost, The theory of two-electron atoms: between ground state and complete fragmentation, *Rev. Mod. Phys.* **72**, 497 (2000).
- [15] R. Wehlitz, Simultaneous emission of multiple electrons from atoms and molecules using synchrotron radiation, *Adv. At. Mol. Opt. Phys.* **58**, 1 (2010).
- [16] J. Hozzowska, A. K. Kheifets, J.-C. Dousse, M. Berset, I. Bray, W. Cao, K. Fennane, Y. Kayser, M. Kavčič, J. Szlachetko, and M. Szlachetko, Physical mechanisms

- and scaling laws of K -shell double photoionization, *Phys. Rev. Lett.* **102**, 073006 (2009).
- [17] J. Hozzowska and J.-C. Dousse, Photoinduced K -shell hollow atoms, *J. Electron. Spectrosc. Relat. Phenom.* **188**, 62 (2013).
- [18] V. A. Zaytsev, I. A. Maltsev, I. I. Tupitsyn, and V. M. Shabaev, Complex-scaled relativistic configuration-interaction study of the LL resonances in heliumlike ions: From boron to argon, *Phys. Rev. A* **100**, 052504 (2019).
- [19] K. N. Lyashchenko, O. Y. Andreev, and D. Yu, QED calculation of two-electron one-photon transition probabilities in He-like ions, *Phys. Rev. A* **104**, 012818 (2021).
- [20] C. Wu, X. Ding, M. Cao, D. Zhang, M. Zhang, Y. Xue, D. Yu, and C. Dong, Energy levels and radiative transition properties of the $2s2p$ double K -shell vacancy state in He-like ions ($4 \leq Z \leq 54$), *At. Data Nucl. Data* **154**, 101602 (2023).
- [21] P. M. Becker and J. S. Dahler, Double excitation of helium by electron impact, *Phys. Rev.* **136**, A73 (1964).
- [22] W. B. Westerveld, F. B. Kets, H. G. M. Heideman, and J. van Eck, Electron impact excitation of the $(2p^2) \ ^3P$ doubly excited state of helium, *J. Phys. B: Atom. Mol. Phys.* **12**, 2575 (1979).
- [23] B. Padhy and D. K. Rai, Two-electron excitation in helium-like ions by electron impact, *Pramana - J. Phys.* **35**, 341 (1990).
- [24] A. Mikhailov, I. Mikhailov, A. Nefiodov, and G. Plunien, Excitation of autoionizing states of helium-like ions by scattering of high-energy particles, *J. Exp. Theor. Phys.* **116**, 363 (2013).
- [25] C. W. Woods, R. L. Kauffman, K. A. Jamison, N. Stolterfoht, and P. Richard, K -shell Auger-electron hypersatellites of Ne, *Phys. Rev. A* **12**, 1393 (1975).
- [26] M. Rødbro, R. Bruch, and P. Bisgaard, High-resolution projectile Auger spectroscopy for Li, Be, B and C excited in single gas collisions I. line energies for prompt decay, *J. Phys. B: At. Mol. Opt. Phys.* **12**, 2413 (1979).
- [27] M. Mack, J. H. Nijland, P. van der Straten, A. Niehaus, and R. Morgenstern, Correlation in double electron capture in collisions of fully stripped ions on He and H₂, *Phys. Rev. A* **39**, 3846 (1989).
- [28] M. Barat and P. Roncin, Multiple electron capture by highly charged ions at keV energies, *J. Phys. B: At. Mol. Opt. Phys.* **25**, 2205 (1992).
- [29] E. P. Benis, T. J. M. Zouros, T. W. Gorczyca, A. D. González, and P. Richard, Elastic resonant and nonresonant differential scattering of quasifree electrons from B⁴⁺(1s) and B³⁺(1s²) ions, *Phys. Rev. A* **69**, 052718 (2004).
- [30] R. Bruch, G. Paul, J. Andrä, and L. Lipsky, Autoionization of foil-excited states in Li I and Li II, *Phys. Rev. A* **12**, 1808 (1975).
- [31] S. Kasthurirangan, J. K. Saha, A. N. Agnihotri, S. Bhattacharyya, D. Misra, A. Kumar, P. K. Mukherjee, J. P. Santos, A. M. Costa, P. Indelicato, T. K. Mukherjee, and L. C. Tribedi, Observation of $2p3d \ ^1P^o \rightarrow 1s3d \ ^1D^e$ radiative transition in He-like Si, S, and Cl ions, *Phys. Rev. Lett.* **111**, 243201 (2013).
- [32] E. T. Kennedy, J. T. Costello, J. P. Mosnier, and P. van Kampen, VUV/EUV ionising radiation and atoms and ions: dual laser plasma investigations, *Rad. Phys. Chem.* **70**, 291 (2004).
- [33] G. Kilgus, J. Berger, P. Blatt, M. Grieser, D. Habs, B. Hochadel, E. Jaeschke, D. Krämer, R. Neumann, G. Neureither, W. Ott, D. Schwalm, M. Steck, R. Stokstad, E. Szmola, A. Wolf, R. Schuch, A. Müller, and M. Wagner, Dielectronic recombination of hydrogenlike oxygen in a heavy-ion storage ring, *Phys. Rev. Lett.* **64**, 737 (1990).
- [34] D. R. DeWitt, E. Lindroth, R. Schuch, H. Gao, T. Quinteros, and W. Zong, Spectroscopy of highly doubly-excited states of helium through dielectronic recombination, *J. Phys. B: At. Mol. Opt. Phys.* **28**, L147 (1995).
- [35] D. Bernhardt, C. Brandau, Z. Harman, C. Kozhuharov, A. Müller, W. Scheid, S. Schippers, E. W. Schmidt, D. Yu, A. N. Artemyev, I. I. Tupitsyn, S. Böhm, F. Bosch, F. J. Currell, B. Franzke, A. Gumberidze, J. Jacobi, P. H. Mokler, F. Nolden, U. Spillman, Z. Stachura, M. Steck, and T. Stöhlker, Breit interaction in dielectronic recombination of hydrogenlike uranium, *Phys. Rev. A* **83**, 020701(R) (2011).
- [36] S.-X. Wang, C. Brandau, S. Fritzsche, S. Fuchs, Z. Harman, C. Kozhuharov, A. Müller, M. Steck, and S. Schippers, Breit interaction in dielectronic recombination of hydrogenlike xenon ions: Storage-ring experiment and theory, *Eur. Phys. J. D* **78**, 122 (2024).
- [37] A. Müller, A. Borovik Jr., K. Huber, S. Schippers, D. V. Fursa, and I. Bray, Double- K -vacancy states in electron-impact single ionization of metastable two-electron N⁷⁺(1s2s ³S₁) ions, *Phys. Rev. A* **90**, 010701(R) (2014).
- [38] A. Müller, A. Borovik Jr., K. Huber, S. Schippers, D. V. Fursa, and I. Bray, Indirect contributions to electron-impact ionization of Li⁺(1s2s ³S₁) ions: Role of intermediate double- K -vacancy states, *Phys. Rev. A* **97**, 022709 (2018).
- [39] S. Diehl, D. Cubaynes, J.-M. Bizau, F. J. Wuilleumier, E. T. Kennedy, J.-P. Mosnier, and T. J. Morgan, New high-resolution measurements of doubly excited states of Li⁺, *J. Phys. B: At. Mol. Opt. Phys.* **32**, 4193 (1999).
- [40] P. K. Carroll and E. T. Kennedy, Doubly excited autoionization resonances in the absorption spectrum of Li⁺ formed in a laser-produced plasma, *Phys. Rev. Lett.* **38**, 1068 (1977).
- [41] L. M. Kiernan, E. T. Kennedy, J.-P. Mosnier, J. T. Costello, and B. F. Sonntag, First observation of a photon induced triply excited state in atomic lithium, *Phys. Rev. Lett.* **72**, 2359 (1994).
- [42] E. Jannitti, P. Nicolosi, and G. Tondello, Photoionization and double excitation spectrum of Be²⁺, *Opt. Commun.* **50**, 225 (1984).
- [43] S. W. J. Scully, I. Álvarez, C. Cisneros, E. D. Emmons, M. F. Gharaibeh, D. Leitner, M. S. Lubell, A. Müller, R. A. Phaneuf, R. Püttner, A. S. Schlachter, S. Schippers, and B. M. McLaughlin, Doubly excited resonances in the photoionization spectrum of Li⁺: Experiment and theory, *J. Phys. B: At. Mol. Opt. Phys.* **39**, 3957 (2006).
- [44] A. Müller, E. Lindroth, S. Bari, A. Borovik, Jr., P.-M. Hillenbrand, K. Holste, P. Indelicato, A. L. D. Kilcoyne, S. Klumpp, M. Martins, J. Viefhaus, P. Wilhelm, and S. Schippers, Photoionization of metastable heliumlike C⁴⁺(1s2s ³S₁) ions: Precision study of intermediate doubly excited states, *Phys. Rev. A* **98**, 033416 (2018).
- [45] J. Viefhaus, F. Scholz, S. Deinert, L. Glaser, M. Ilchen, J. Seltmann, P. Walter, and F. Siewert, The variable po-

- larization XUV beamline P04 at PETRA III: optics, mechanics and their performance, *Nucl. Instrum. Methods Phys. Res.* **A710**, 151 (2013).
- [46] C. G. Schroer, H.-C. Wille, O. H. Seeck, K. Bagschik, H. Schulte-Schrepping, M. Tischer, H. Graafsma, W. Laasch, K. Baev, S. Klumpp, R. Bartolini, H. Reichert, W. Leemans, and E. Weckert, The synchrotron radiation source PETRA III and its future ultra-low-emittance upgrade PETRA IV, *Eur. Phys. J. Plus* **137**, 1312 (2022).
- [47] S. Schippers, T. Buhr, A. Borovik Jr., K. Holste, A. Perry-Sassmannshausen, K. Mertens, S. Reinwardt, M. Martins, S. Klumpp, K. Schubert, S. Bari, R. Beerwerth, S. Fritzsche, S. Ricz, J. Hellhund, and A. Müller, The photon-ion merged-beams experiment PIPE at PETRA III - The first five years, *X-Ray Spectrom.* **49**, 11 (2020).
- [48] R. A. Phaneuf, C. C. Havener, G. H. Dunn, and A. Müller, Merged-beams experiments in atomic and molecular physics, *Rep. Prog. Phys.* **62**, 1143 (1999).
- [49] S. Schippers, S. Ricz, T. Buhr, A. Borovik Jr., J. Hellhund, K. Holste, K. Huber, H.-J. Schäfer, D. Schury, S. Klumpp, K. Mertens, M. Martins, R. Flesch, G. Ulrich, E. Rühl, T. Jahnke, J. Lower, D. Metz, L. P. H. Schmidt, M. Schöffler, J. B. Williams, L. Glaser, F. Scholz, J. Seltmann, J. Viefhaus, A. Dorn, A. Wolf, J. Ullrich, and A. Müller, Absolute cross sections for photoionization of Xe^{q+} ions ($1 \leq q \leq 5$) at the $3d$ ionization threshold, *J. Phys. B: At. Mol. Opt. Phys.* **47**, 115602 (2014).
- [50] A. Müller, D. Bernhardt, A. Borovik Jr., T. Buhr, J. Hellhund, K. Holste, A. L. D. Kilcoyne, S. Klumpp, M. Martins, S. Ricz, J. Seltmann, J. Viefhaus, and S. Schippers, Photoionization of Ne atoms and Ne^+ ions near the K edge: Precision spectroscopy and absolute cross-sections, *Astrophys. J.* **836**, 166 (2017).
- [51] F. Brötz, R. Trassl, R. W. McCullough, W. Arnold, and E. Salzborn, Design of compact all-permanent magnet electron cyclotron resonance (ECR) ion sources for atomic physics experiments, *Phys. Scr.* **T92**, 278 (2001).
- [52] G. W. F. Drake, Theory of relativistic magnetic dipole transitions: Lifetime of the metastable 2^3S state of the heliumlike ions, *Phys. Rev. A* **3**, 908 (1971).
- [53] A. C. Renwick, I. Bray, D. V. Fursa, J. Jacobi, H. Knopp, S. Schippers, and A. Müller, Electron-impact ionization of B^{3+} ions, *J. Phys. B: At. Mol. Opt. Phys.* **42**, 175203 (2009).
- [54] A. Derevianko and W. R. Johnson, Two-photon decay of 2^1S_0 and 2^3S_1 states of heliumlike ions, *Phys. Rev. A* **56**, 1288 (1997).
- [55] V. A. Yerokhin, V. Patkóš, and K. Pachucki, QED calculations of energy levels of heliumlike ions with $5 \leq Z \leq 30$, *Phys. Rev. A* **106**, 022815 (2022).
- [56] R. N. S. Sodhi and C. E. Brion, Reference energies for inner shell electron energy-loss spectroscopy, *J. Elec. Spectrosc. Relat. Phenom.* **34**, 363 (1984).
- [57] J. Stierhof, S. Kühn, M. Winter, P. Micke, R. Steinbrügge, C. Shah, N. Hell, M. Bissinger, M. Hirsch, R. Ballhausen, M. Lang, C. Gräfe, S. Wipf, R. Cumbee, G. L. Betancourt-Martinez, S. Park, J. Niskanen, M. Chung, F. S. Porter, T. Stöhlker, T. Pfeifer, G. V. Brown, S. Bernitt, P. Hansmann, J. Wilms, J. R. C. López-Urrutia, and M. A. Leutenegger, A new benchmark of soft x-ray transition energies of Ne, CO_2 , and SF_6 : paving a pathway towards ppm accuracy, *Eur. Phys. J. D* **76**, 38 (2022).
- [58] S. Salomonson and P. Öster, Relativistic all-order pair functions from a discretized single-particle Dirac Hamiltonian, *Phys. Rev. A* **40**, 5548 (1989).
- [59] I. Lindgren, The Rayleigh-Schrödinger perturbation and the linked-diagram theorem for a multi-configurational model space, *J. Phys. B: At. Mol. Opt. Phys.* **7**, 2441 (1974).
- [60] E. Lindroth, Calculation of doubly excited states of helium with a finite discrete spectrum, *Phys. Rev. A* **49**, 4473 (1994).
- [61] M. Lestinsky, E. Lindroth, D. A. Orlov, E. W. Schmidt, S. Schippers, S. Böhm, C. Brandau, F. Sprenger, A. S. Terekhov, A. Müller, and A. Wolf, Screened radiative corrections from hyperfine-split dielectronic resonances in lithiumlike scandium, *Phys. Rev. Lett.* **100**, 033001 (2008).
- [62] M. Tokman, N. Eklöv, P. Glans, E. Lindroth, R. Schuch, G. Gwinner, D. Schwalm, A. Wolf, A. Hoffknecht, A. Müller, and S. Schippers, Dielectronic recombination resonances in F^{6+} , *Phys. Rev. A* **66**, 012703 (2002).
- [63] E. Lindroth and L. Argenti, Atomic resonance states and their role in charge-changing processes, *Adv. Quantum Chem.* **63**, 247 (2012).
- [64] V. A. Yerokhin and V. M. Shabaev, Lamb shift of $n = 1$ and $n = 2$ states of hydrogen-like atoms, $1 \leq Z \leq 110$, *J. Phys. Chem. Ref. Data* **44**, 033103 (2015).
- [65] D. S. Hughes and C. Eckart, The effect of the motion of the nucleus on the spectra of Li I and Li II, *Phys. Rev.* **36**, 694 (1930).
- [66] A. S. Kheifets and I. Bray, Calculation of double photoionization of helium using the convergent close-coupling method, *Phys. Rev. A* **54**, R995 (1996).
- [67] A. S. Kheifets and I. Bray, Photoionization with excitation and double photoionization of the helium isoelectronic sequence, *Phys. Rev. A* **58**, 4501 (1998).
- [68] I. Bray, D. V. Fursa, A. S. Kheifets, and A. T. Stelbovics, Electrons and photons colliding with atoms: development and application of the convergent close-coupling method, *J. Phys. B: At. Mol. Opt. Phys.* **35**, R117 (2002).
- [69] A. W. Bray, A. S. Kheifets, and I. Bray, Calculation of atomic photoionization using the nonsingular convergent close-coupling method, *Phys. Rev. A* **95**, 053405 (2017).
- [70] R. D. Cowan, *The Theory of Atomic Structure and Spectra* (University of California Press, Berkeley, 1981).
- [71] M. Martins, Photoionization of open-shell atoms: the chlorine 2p excitation, *J. Phys. B: At. Mol. Opt. Phys.* **34**, 1321 (2001).
- [72] D. Pines, Emergent behavior in strongly correlated electron systems, *Rep. Prog. Phys.* **79**, 092501 (2016).
- [73] G. Co', Introducing the random phase approximation theory, *Universe* **9**, 141 (2023).
- [74] M. Y. Amusia, Atomic photoeffect, in *Physics of Atoms and Molecules*, edited by K. T. Taylor (Plenum Press, New York, 1990).
- [75] M. Y. Amusia, Random phase approximation: From giant to intra-doublet resonances, *Rad. Phys. Chem.* **70**, 237 (2004).
- [76] K. L. Bell and A. E. Kingston, Photoionization cross sections for the heliumisoelectronic series, *J. Phys. B: At. Mol. Opt. Phys.* **4**, 1308 (1971).

- [77] R. F. Reilman and S. T. Manson, Photoabsorption cross sections for positive atomic ions with $Z \leq 30$, *Astrophys. J. Suppl. Ser.* **40**, 815 (1979).
- [78] D. A. Verner, D. G. Yakovlev, I. M. Band, and M. B. Trzhaskovskaya., Subshell photoionization cross sections and ionization energies of atoms and ions from He to Zn, *At. Data Nucl. Data Tables* **55**, 233 (1993).
- [79] A. Mikhailov, A. Nefiodov, and G. Plunien, Single photoeffect on helium-like ions in the non-relativistic region, *Physics Letters A* **368**, 391 (2007).
- [80] M. Stobbe, Zur Quantenmechanik photoelektrischer Prozesse, *Ann. Phys. (Leipzig)* **7**, 661 (1930).
- [81] U. Fano, Effects of configuration interaction on intensities and phase shifts, *Phys. Rev.* **124**, 1866 (1961).
- [82] D. R. Herrick and O. Sinanoğlu, Comparison of doubly-excited helium energy levels, isoelectronic series, autoionization lifetimes, and group-theoretical configuration-mixing predictions with large-configuration-interaction calculations and experimental spectra, *Phys. Rev. A* **11**, 97 (1975).
- [83] C. D. Lin, Classification of doubly excited states of two-electron atoms, *Phys. Rev. Lett.* **51**, 1348 (1983).
- [84] C. D. Lin, Classification and supermultiplet structure of doubly excited states, *Phys. Rev. A* **29**, 1019 (1984).
- [85] C. D. Lin, Hyperspherical coordinate approach to atomic and other Coulombic three-body systems, *Phys. Rep.* **257**, 1 (1995).
- [86] M. Domke, C. Xue, A. Puschnann, T. Mandel, E. Hudson, D. A. Shirley, G. Kaindl, C. H. Greene, H. R. Sadeghpour, and H. Petersen, Extensive double-excitation states in atomic helium, *Phys. Rev. Lett.* **66**, 1306 (1991).
- [87] M. Domke, G. Remmers, and G. Kaindl, Observation of the $(2p, nd) \ ^1P^o$ double-excitation Rydberg series of helium, *Phys. Rev. Lett.* **69**, 1171 (1992).
- [88] K. Schulz, G. Kaindl, M. Domke, J. D. Bozek, P. A. Heimann, A. S. Schlachter, and J. M. Rost, Observation of new Rydberg series and resonances in doubly excited helium at ultrahigh resolution, *Phys. Rev. Lett.* **77**, 3086 (1996).
- [89] R. Püttner, B. Grémaud, D. Delande, M. Domke, M. Martins, A. S. Schlachter, and G. Kaindl, Statistical properties of inter-series mixing in helium: From integrability to chaos, *Phys. Rev. Lett.* **86**, 3747 (2001).
- [90] E. T. Kennedy and P. K. Carroll, Satellite lines of low-Z elements (Li, Be, B) observed in laser-produced plasmas, *J. Phys. B: At. Mol. Opt. Phys.* **11**, 965 (1978).
- [91] Y. Gning, M. Sow, A. Traoré, M. Dieng, B. Diakhate, M. Biaye, and A. Wagué, Calculations of resonance parameters for the $((2s^2) \ ^1S^e, (2s2p) \ ^{1,3}P^o)$ and $((3s^2) \ ^1S^e, (3s3p) \ ^{1,3}P^o)$ doubly excited states of helium-like ions with $Z \leq 10$ using a complex rotation method implemented in Scilab, *Rad. Phys. Chem.* **106**, 1 (2015).
- [92] S. Schippers, Analytical expression for the convolution of a Fano line profile with a Gaussian, *J. Quant. Spectrosc. Radiat. Transfer* **219**, 33 (2018).
- [93] R. Reininger and A. R. B. de Castro, High resolution, large spectral range, in variable-included-angle soft x-ray monochromators using a plane VLS grating, *Nucl. Instrum. Methods A* **538**, 760 (2005).